Resource

Immunity

Single-cell functional genomics reveals determinants of sensitivity and resistance to natural killer cells in blood cancers

Graphical abstract

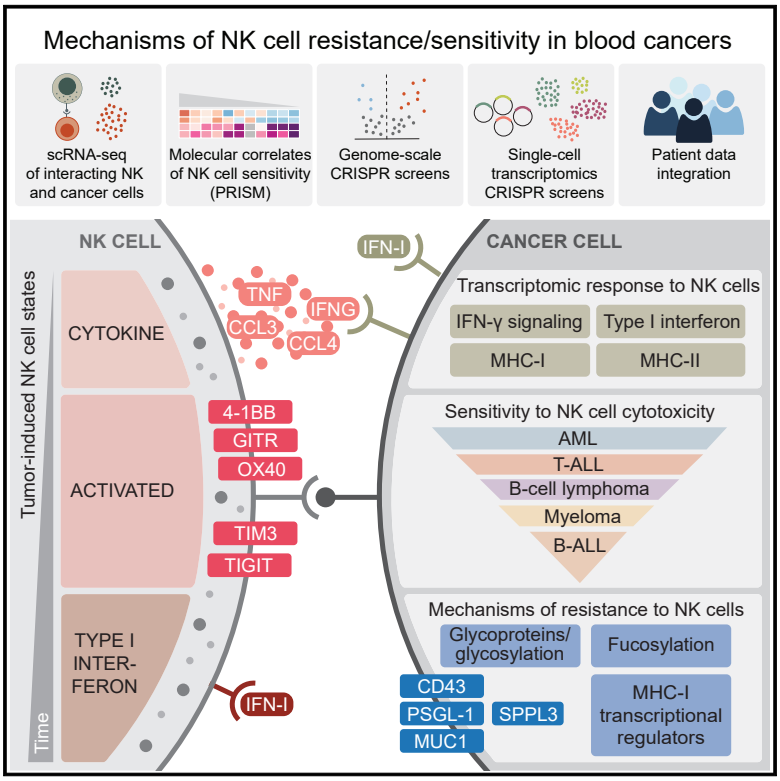

Highlights

- Tumor-NK cell interaction triggers transcriptional states dictated by tumor features
- CRISPR and PRISM screens reveal cancer subtype-specific NK cell evasion mechanisms
- NK resistance genes include *SELPLG*, *SPN*, *MUC1*, *FUT8*, and *GMDS*
- Single-cell CRISPR screens identify MHC-I, IFN-γ, and NF-κB regulation as mechanisms

Authors

Olli Dufva, Sara Gandolfi, Jani Huuhtanen, ..., Matti Kankainen, Constantine S. Mitsiades, Satu Mustjoki

Correspondence

constantine_mitsiades@dfci.harvard.edu (C.S.M.), satu.mustjoki@helsinki.fi (S.M.)

In brief

Natural killer (NK) cells are an emerging immunotherapy, particularly in blood cancers. Dufva, Gandolfi et al. examined interacting NK and a broad panel of blood cancer types using single-cell transcriptomics and CRISPR screens. Their findings reveal various mechanisms of NK cell resistance, as well as potential targets to augment NK cell-based immunotherapies.

Dufva et al., 2023, Immunity *56*, 2816–2835
December 12, 2023
https://doi.org/10.1016/j.immuni.2023.11.008

CellPress

CellPress
OPEN ACCESS

Immunity

Resource

Single-cell functional genomics reveals determinants of sensitivity and resistance to natural killer cells in blood cancers

Olli Dufva,[1,2,3,15] Sara Gandolfi,[1,2,3,4,5,15] Jani Huuhtanen,[1,2,3,12,16] Olga Dashevsky,[4,5,6,7,16] Hanna Duàn,[1,2,3,16] Khalid Saeed,[1,2] Jay Klievink,[1,2,3] Petra Nygren,[1,2,3] Jonas Bouhlal,[1,2,3] Jenni Lahtela,[8] Anna Näätänen,[8] Bishwa R. Ghimire,[8] Tiina Hannunen,[8] Pekka Ellonen,[8] Hanna Lähteenmäki,[1,2] Pauliina Rumm,[1,2] Jason Theodoropoulos,[1,2] Essi Laajala,[1,2,3] Jouni Härkönen,[9] Petri Pölönen,[10] Merja Heinäniemi,[9] Maija Hollmén,[11] Shizuka Yamano,[4,5,6,7] Ryosuke Shirasaki,[4,5,6,7] David A. Barbie,[4,5,6,7] Jennifer A. Roth,[5] Rizwan Romee,[4,6,7] Michal Sheffer,[4,5,6,7] Harri Lähdesmäki,[12] Dean A. Lee,[13] Ricardo De Matos Simoes,[4,5,6,7] Matti Kankainen,[1,2,3,14] Constantine S. Mitsiades,[4,5,6,7,17,18,*] and Satu Mustjoki[1,2,3,17,18,*]

[1]Hematology Research Unit Helsinki, Helsinki University Hospital Comprehensive Cancer Center, 00290 Helsinki, Finland
[2]Translational Immunology Research Program and Department of Clinical Chemistry and Hematology, University of Helsinki, 00014 Helsinki, Finland
[3]iCAN Digital Precision Cancer Medicine Flagship, 00290 Helsinki, Finland
[4]Department of Medical Oncology, Dana-Farber Cancer Institute, Harvard Medical School, Boston, MA 02215, USA
[5]Broad Institute of MIT and Harvard, Cambridge, MA 02142, USA
[6]Department of Medicine, Harvard Medical School, Boston, MA 02215, USA
[7]Ludwig Center, Harvard Medical School, Boston, MA 02215, USA
[8]Institute for Molecular Medicine Finland (FIMM), HiLIFE, University of Helsinki, 00014 Helsinki, Finland
[9]Faculty of Health Sciences, A.I. Virtanen Institute for Molecular Sciences, University of Eastern Finland, 70211 Kuopio, Finland
[10]Department of Pathology, St. Jude Children's Research Hospital, Memphis, TN 38105, USA
[11]Medicity Research Laboratory, University of Turku, 20014 Turku, Finland
[12]Department of Computer Science, Aalto University, 02150 Espoo, Finland
[13]Hematology/Oncology/BMT, Center for Childhood Cancer and Blood Diseases, Nationwide Children's Hospital, Columbus, OH 43205, USA
[14]Laboratory of Genetics, HUS Diagnostic Center, Hospital District of Helsinki and Uusima (HUS), 00290 Helsinki, Finland
[15]These authors contributed equally
[16]These authors contributed equally
[17]Senior author
[18]Lead contact
*Correspondence: constantine_mitsiades@dfci.harvard.edu (C.S.M.), satu.mustjoki@helsinki.fi (S.M.)
https://doi.org/10.1016/j.immuni.2023.11.008

SUMMARY

Cancer cells can evade natural killer (NK) cell activity, thereby limiting anti-tumor immunity. To reveal genetic determinants of susceptibility to NK cell activity, we examined interacting NK cells and blood cancer cells using single-cell and genome-scale functional genomics screens. Interaction of NK and cancer cells induced distinct activation and type I interferon (IFN) states in both cell types depending on the cancer cell lineage and molecular phenotype, ranging from more sensitive myeloid to less sensitive B-lymphoid cancers. CRISPR screens in cancer cells uncovered genes regulating sensitivity and resistance to NK cell-mediated killing, including adhesion-related glycoproteins, protein fucosylation genes, and transcriptional regulators, in addition to confirming the importance of antigen presentation and death receptor signaling pathways. CRISPR screens with a single-cell transcriptomic readout provided insight into underlying mechanisms, including regulation of IFN-γ signaling in cancer cells and NK cell activation states. Our findings highlight the diversity of mechanisms influencing NK cell susceptibility across different cancers and provide a resource for NK cell-based therapies.

INTRODUCTION

Natural killer (NK) cells are cytotoxic innate lymphoid cells that can directly eliminate cancer cells,[1] depending on the balance between activating and inhibitory signals derived from surface receptors engaged with cognate ligands on target cells.[2] Data supporting the role of NK cells in graft-versus-leukemia effect in allogeneic hematopoietic stem cell transplantation[3] and the effectiveness of chimeric antigen receptor (CAR) NK cells[4] highlight their promise in blood cancers.[5,6]

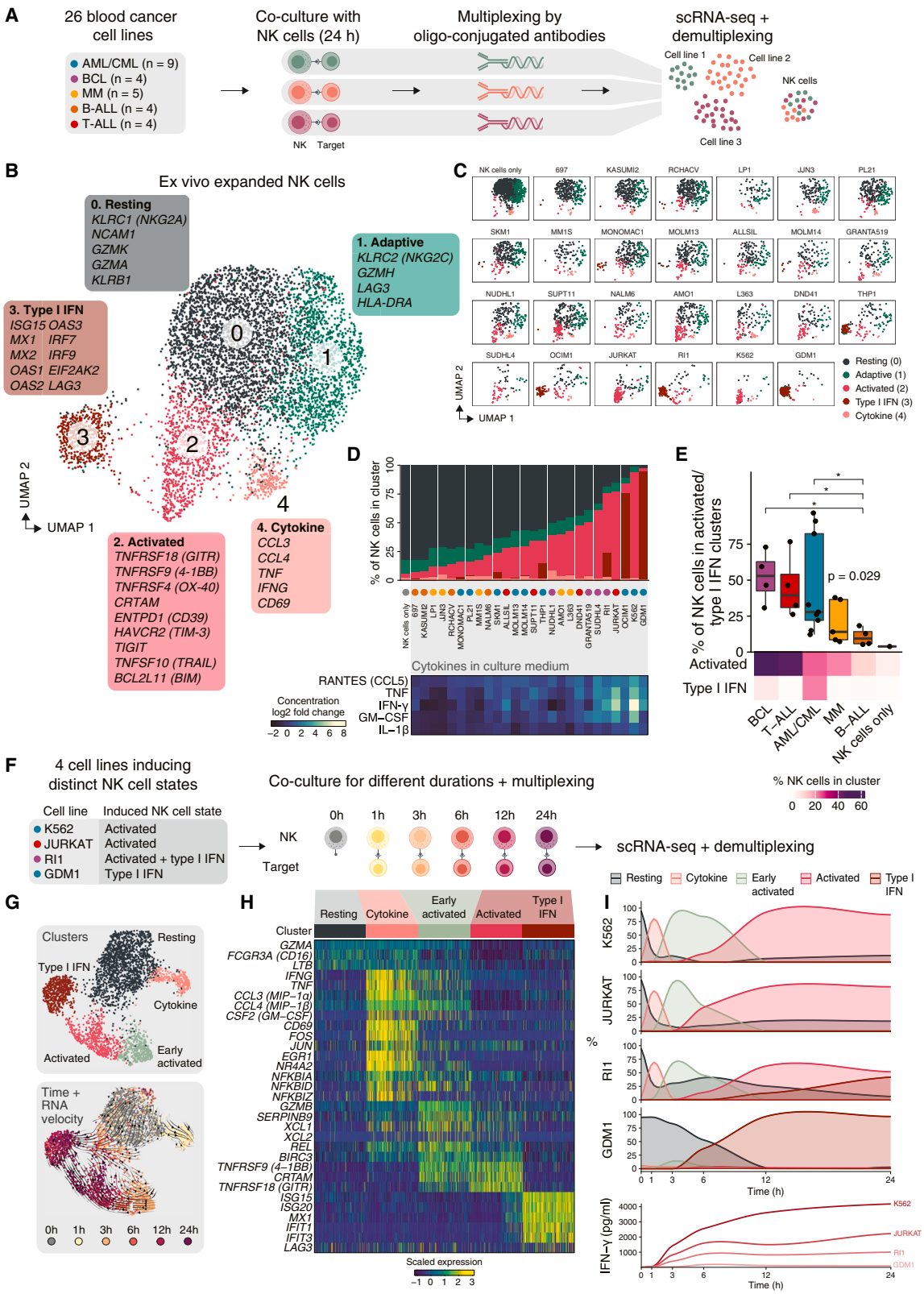

Figure 1. Single-cell transcriptomics of NK cells interacting with blood cancer cells

(A) Multiplexed co-culture scRNA-seq workflow.

(B and C) UMAP of expanded NK cells (donor NK1) from all co-culture and monoculture conditions (B) and separately for each tumor cell line (C).

(legend continued on next page)

Single-cell analyses have unveiled immune cell transcriptional profiles in healthy and cancerous tissues, along with tumor cell transcriptional programs.[7–13] Yet the dynamic changes during tumor-immune interactions remain underexplored at a transcriptomic level. Genome-scale CRISPR screens have revealed cancer cell-intrinsic mechanisms of evasion from T cell killing in solid tumors[14–17] and hematological malignancies.[18,19] CRISPR and PRISM (profiling relative inhibition simultaneously in mixtures) screens[20] have identified molecular factors regulating solid tumor cell sensitivity to NK cell-mediated killing.[21] However, a more systematic evaluation of resistance and sensitivity to NK cell therapies across hematological malignancies is warranted.

Many critical questions remain about harnessing NK cells as effective therapies. We need to understand how NK and cancer cells alter their transcriptomes upon interaction, whether these changes and sensitivity to NK cells vary depending on genetic and epigenetic traits in tumor cells and which mechanisms drive tumor resistance toward NK cells. Linking cancer subtypes to NK cell sensitivity can identify those who may benefit from treatment and uncover novel approaches to target resistant cancers.

Here, we sought to answer these questions by combining multiplexed single-cell RNA sequencing (scRNA-seq) of interacting NK cells and cancer cells, PRISM-based profiling of NK cell sensitivity across a panel of blood cancer cell lines, and genome-scale and single-cell transcriptomic CRISPR screens of cancer-cell intrinsic NK cell resistance mechanisms. By integrating these data and patient genomic profiles, we provide a comprehensive landscape of functionally validated molecular mechanisms that influence how NK cells recognize and kill malignant hematopoietic cells. The results offer a roadmap to facilitate the development of NK cell-based immunotherapy for blood cancers and beyond. The data are available for interactive exploration at https://immunogenomics.shinyapps.io/nkheme/.

RESULTS

Cancer cell interaction-induced phenotypic changes in NK cells

Defining how the state of NK and cancer cells may change upon their interaction is essential for understanding potential mechanisms of adaptive, interaction-induced resistance. We therefore cultured 26 cell lines representing diverse hematologic neoplasms either alone or with donor-derived (n = 3) *ex vivo*-expanded or non-expanded NK cells. The cancer types included acute and chronic myeloid leukemia (AML and CML), B and T cell acute lymphoblastic leukemia (B-ALL and T-ALL), B cell lymphoma (BCL), and multiple myeloma (MM). After 24 h co-culture, we performed scRNA-seq using cell hashing,[22] obtaining a total of 128,621 cells across 193 samples (666 cells per sample on average) (Figure S1A; Table S1).

Unsupervised clustering of the *ex vivo*-expanded NK cells (donor NK1) in all conditions revealed five clusters (Figures 1B and S1B). Most monocultured NK cells belonged to two clusters: resting NK cells (cluster 0) expressing markers of CD56bright NK cells (*NCAM1/CD56*, *KLRC1/NKG2A*, *GZMK*),[7–10] consistent with the CD56bright phenotype of expanded NK cells,[23,24] and adaptive NK cells (cluster 1) based on expression of *KLRC2/NKG2C* and *LAG3*[25,26] (Figure 1B). By contrast, the remaining three NK cell clusters (2, 3, and 4) were mostly enriched in the co-culture conditions with tumor cells. NK cells with an activated phenotype (cluster 2) expressed co-stimulatory (*TNFRSF18/GITR*, *TNFRSF9/4-1BB*, *TNFRSF4/OX-40*, and *CRTAM*) and inhibitory receptor genes (*HAVRC2/TIM-3* and *TIGIT*), immediate-early genes (*DUSP2*, *DUSP4*, and *EGR2*), the death receptor ligand gene *TNFSF10/TRAIL*, and *ENTPD1/CD39* gene associated with tumor-reactive T cells and exhaustion.[27–29] Other clusters enriched upon target cell encounter included NK cells with high type I interferon (IFN-I) signature (cluster 3) expressing antiviral genes (*MX1-2* and *OAS1-3*) and the inhibitory receptor gene *LAG3*, and cytokine-producing NK cells (cluster 4) expressing *CCL3/MIP-1α*, *CCL4/MIP-1β*, *TNF, IFNG*, and *CSF2/GM-CSF*.

Different cell lines triggered distinct NK cell phenotypic changes. For instance, K562 (CML), JURKAT (T-ALL), and SUDHL4 (BCL) induced over 50% of NK cells into the activated state, compared with less than 20% with several B-ALL and MM cell lines (Figures 1C and 1D). The IFN-I state was only induced by certain cell lines, including GDM1, OCIM1, THP1 (AML), and RI1 (BCL). The tumor-induced NK cell activation states correlated with secreted cytokines, including IFN-γ, TNF, CCL5, and GM-CSF, consistent with the states representing actively functioning NK cells[30–32] (Figure 1D).

The percentages of activated and IFN-I state NK cells across all 26 co-culture conditions were consistent in the three donors (Figures S1C and S1D) and also in a panel of six donors representing different HLA (human leukocyte antigen)-C genotypes (Figure S1D). Instead, the responses varied by cancer type, with stronger responses against BCL, T-ALL, and AML/CML compared with B-ALL (Figure 1E).

NK cells from unexpanded peripheral blood mononuclear cells (PBMCs) showed concordant tumor-induced responses, underscoring the relevance of these activation states to circulating NK cells (Figures S1E–S1H). In non-expanded NK cells, however, the cytokine state was more prominently induced by co-culture (Figure S1H).

To monitor the evolution of the responses observed at 24 h, we performed serial scRNA-seq at 1–24 h after co-culture start (Figures 1F–1I and S1I). At 1 h, most NK cells transitioned to

(D) Bar plot of average percentages of NK cell clusters across three NK donors (top). Heatmap of cytokines whose concentration increases in co-cultures correlate the most with tumor-induced NK cell states (bottom).
(E) Boxplot of percentages of NK cells in activated or IFN-I states. Boxes indicate interquartile range (IQR) with a line at the median. Whiskers represent the min and max values at most 1.5 IQR from the quartiles. Below, heatmap of median percentages of NK cells in activated or IFN-I states separately.
(F) Time course experiment workflow.
(G) UMAP of expanded NK cells (donor NK1) from all time points co-cultured with the different cell lines colored based on clusters (above) and on time point, with arrows indicating RNA velocity fields (below).
(H) Expression of selected genes enriched in each NK cluster in the time course experiment as a heatmap.
(I) Co-cultures of NK cells with indicated cell lines: time course of NK cell cluster percentages and IFN-γ concentration in co-culture medium.
See also Figure S1 and Table S1.

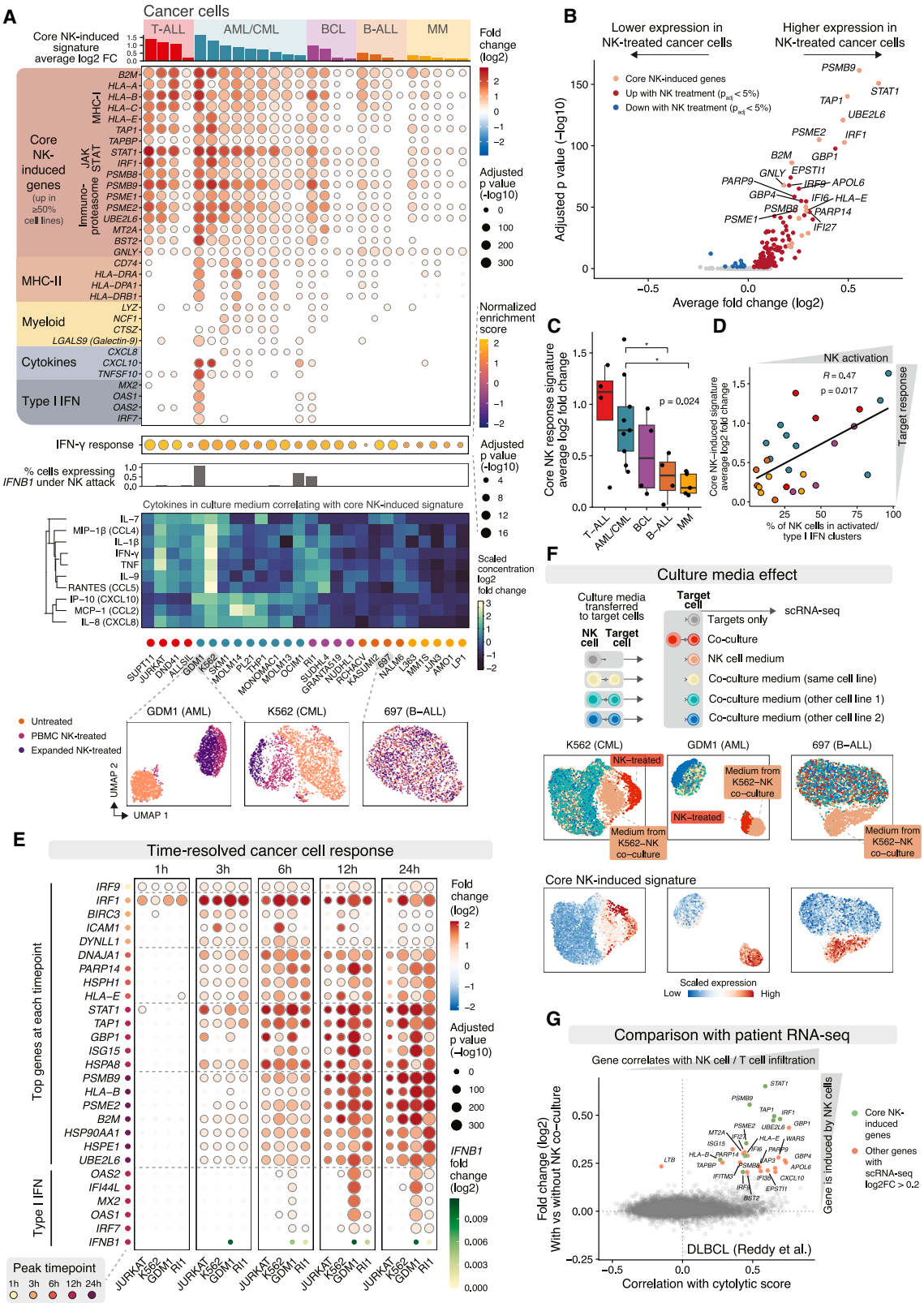

Figure 2. Transcriptomic responses of blood cancer cells to NK cell attack

(A) Dot plot of selected genes upregulated in cancer cells exposed to expanded NK cells. Heatmap shows co-culture-induced cytokine increases with highest correlation with the core NK cell response. At the bottom, examples of UMAPs of selected cell lines.

(legend continued on next page)

the cytokine state (which pre-existed at a minor fraction in unchallenged NK cells), upregulating *CD69*, *IFNG*, *TNF*, *CCL3*, *CCL4*, and *CSF2/GM-CSF*. Concordantly, cytokines, such as IFN-γ, started rising after 1 h in those co-cultures that strongly induced the cytokine state (Figure 1I). Between 3 and 6 h, the NK cells upregulated *GZMB*, *XCL1*, and *XCL2* and started to express hallmarks of the activated phenotype (such as *TNFRSF9* and *CRTAM*), constituting an early activated state (Figures 1G and 1H). The activated signature peaked from 12 h onward, similarly to the IFN-I signature when present (Figure 1I). RNA velocity[33] analysis suggested that the IFN-I state may emerge from both resting and activated cells (Figure 1G). These findings suggest that the 24 h time point measured across the larger cell line panel reflects the maximal tumor-induced activation state and additionally captures the type I IFN state when present.

The IFN-I state could be induced in NK cell monocultures by co-culture-derived media, indicating that secreted factors underlie this response (Figure S1J). By contrast, the activated state could not be evoked by the co-culture medium, implying that cell-cell contact is required. Taken together, NK cells engaging with cancer cells shift into activated states with an altered repertoire of co-stimulatory and co-inhibitory receptors, with the magnitude and direction of the transition depending on the target cells.

Transcriptomic responses of blood cancer cells to NK cell attack

We then examined the transcriptomic responses in cancer cells following NK cell attack. Comparing all expanded NK cell-treated target cells to untreated controls revealed a strong induction of IFN-γ response (Figures 2A, 2B, and S2A; Table S2). A core set of 17 genes significantly induced in at least 50% of the cell lines comprised the class I major histocompatibility complex (MHC-I) genes (*B2M* and HLA-A/B/C/E), MHC-I peptide-loading genes (*TAP1* and *TAPBP*), JAK-STAT signaling genes (*STAT1* and *IRF1*), immunoproteasome genes (*PSMB8, PSMB9, PSME1,* and *PSME2*), and other genes (*UBE2L6*, *MT2A*, *BST2*, and *GNLY*) (Figure 2A). This induced signature was particularly strong in T-ALL, AML, and CML compared with other blood cancers (Figure 2C).

To uncover distinct transcriptional programs induced in subsets of cell lines, we examined the 200 genes most variably induced across cell lines by unsupervised clustering (Figure S2A). This highlighted IFN-γ-associated programs, including the core NK-induced signature and cytokines, such as *CXCL8* (interleukin [*IL*]-*8*), *CXCL10*, and *TNFSF10* (*TRAIL*). Cytokines in the culture media, including NK cell-produced IFN-γ and those produced by cancer cells based on scRNA-seq (IL-8 and CXCL10), consistently correlated with the core NK-induced signature (Figure 2A). MHC class II (MHC-II) genes were induced in monocytic cells and several B cell lines. A myeloid differentiation signature, including *LYZ, NCF1, CTSZ*, and the TIM-3 ligand *LGALS9*, was induced in AML cells, suggesting that NK cell attack may be accompanied by maturation of monocytic leukemias, as reported in response to IFN-γ.[34] NK cell attack induced an IFN-I signature and *IFNB1* (*IFN-β*) expression in GDM1, OCIM1, and R1 cells, mirroring a similar signature in the NK cells and implying a coordinated response to IFN-β in both cell types (Figure 2A). Consistently, NK and target cell activation signatures correlated positively across cell lines (Figure 2D).

We examined target cells from the 24 h time course experiment to temporally resolve the signature development (Figure 2E). The earliest events at 1–3 h included induction of IFN response transcription factor (TF) genes *IRF1* and *IRF9*, nuclear factor (NF)-κB target *BIRC3*, and the adhesion molecule *ICAM1*. *HLA-E* expression peaked at 6 h, whereas the classical MHC-I genes were fully induced at 24 h. When present, IFN-I signature genes emerged at 6 h, coinciding temporally with the IFN-I cluster in NK cells and following *IFNB1* induction at 3 h.

Medium from co-culture of NK and K562 cells induced the core NK cell response in K562 monocultures, pointing to mediation by soluble factors such as IFN-γ (Figure 2F). NK-K562 co-culture medium also induced the IFN-I signature and *IFNB1* expression in GDM1 cells, implying that the IFN-I effect is mediated by soluble factors. NK-K562 co-culture medium also triggered a transcriptional response in 697 B-ALL cells, suggesting that their unresponsiveness to NK cell interaction likely reflects lack of NK cell activation rather than defective IFN-γ responsiveness.

NK cell-induced signatures in cancer cells from these co-cultures were also identified in patient samples. Most of the NK-induced genes, particularly the 17-gene core set, positively correlated with NK and T cell infiltration in diffuse large BCL (DLBCL)[35] and AML[36] patients (Figures 2G and S2C), suggesting similar transcriptomic responses *in vivo*.

We studied potential ligand-receptor interactions induced upon tumor-NK cell engagement using CellPhoneDB.[37] Several predicted interactions were more frequent between the cancer cells and co-culture-related NK cell states (activated, IFN-I, or cytokine) compared with the resting or adaptive states. These included ligands for activating and inhibitory receptor ligands (*TNFSF9-TNFRSF9*, *TNFSF4-TNFRSF4*, *LGALS9-HAVCR2,* and *CD47-SIRPG*), death receptors (*TNFRSF10A/B-TNFSF10* and FAS-FASLG), cytokines (*TGFB1/3-TGFBR2*), and adhesion molecules (ICAM1-aMb2/aXb2 complex and EFNA3/4/5-EPHA4) (Figure S2D). Interactions induced by tumor-NK cell engagement also included those of MHC-I with inhibitory receptors and CXCL10-CXCR3 (Figure S2E). Taken together, the transcriptomic responses of tumor cells to NK cell attack depend on the tumor cell

(B) Volcano plot of differentially expressed genes between all NK-cell treated cancer cell lines (NK donors n = 3) and the same cell lines cultured alone.
(C) Boxplot of the $\log_2$ fold change ($\log_2$FC) of the core NK cell-induced gene score between NK-treated (NK donors n = 3) and untreated cells. Boxplots displayed as in Figure 1E.
(D) Scatter plot of average NK cell activation (after co-culture) versus core NK cell response induction in NK-treated target cells.
(E) Dot plot of transcripts differentially expressed in cancer cells at different time points of co-culture with NK cells (different color and size scale for *IFNB1* due to its lower expression relative to other genes).
(F) Effects of co-culture-conditioned media on cancer cell transcriptomic states as UMAPs with color indicating culture conditions (above) and the core NK cell response signature score (below).
(G) Scatter plot of induction of genes by NK cell co-culture in target cells versus correlation with NK and T cell infiltration (cytolytic score) in DLBCL patient samples from Reddy et al.
See also Figure S2 and Table S2.

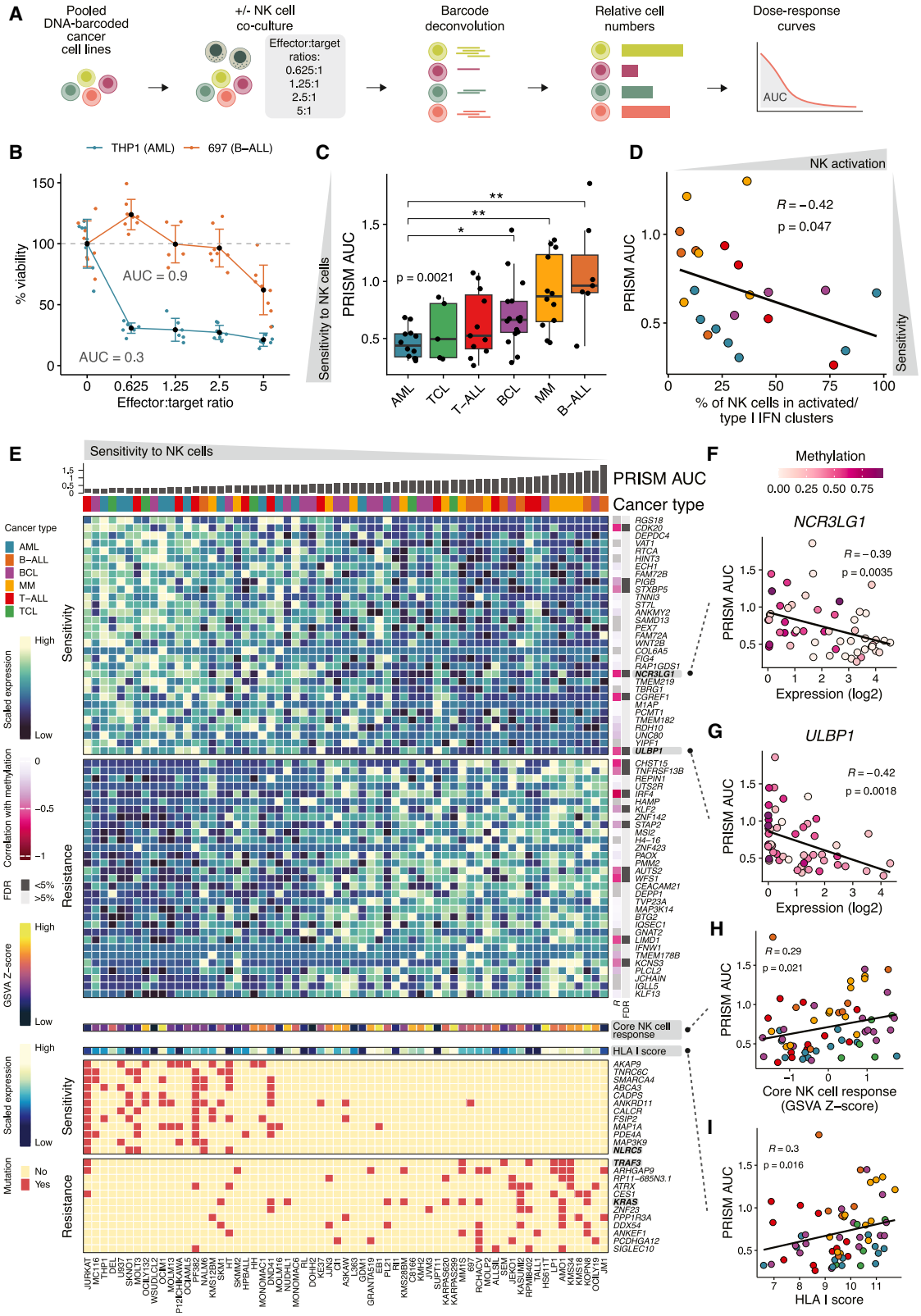

(legend on next page)

lineage and correlate with NK cell activation, resulting in predicted ligand-receptor interactions not found in the resting state.

Molecular correlates of sensitivity to NK cells

To study cancer cell sensitivity to NK cells across different lineages and maturation stages, we quantified the dose-dependent sensitivity of 63 DNA-barcoded blood cancer cell lines to primary NK cells (PRISM system; Figure 3A; Table S3).[20]

We observed substantial heterogeneity in NK cell sensitivity, with AML and B-ALL lines being most and least sensitive, respectively (Figures 3B, 3C, and S3A). MM and T-ALL lines were on average less and more sensitive, respectively, but both showed substantial variation, implying the existence of sensitive and resistant subgroups. The sensitivity correlated with the percentage of NK cells shifting toward activated/IFN-I states (Figures 3D and S3B). Although not all responsive cell lines induced a strong activated/IFN-I state, all resistant cell lines failed to trigger this phenotype (Figure 3D).

We then investigated the molecular factors underlying the variation in NK cell sensitivity by correlating NK cell sensitivity the area under the dose-response curve (AUC) of the PRISM NK cell response data for blood cancer cell lines with their Cancer Cell Line Encyclopedia (CCLE) multi-omics data[38,39] (Figures 3E and S3C). Genes highly correlating with lower AUC (higher sensitivity to NK cells) included the activating receptor ligands *NCR3LG1* and *ULBP1*, whose expression negatively correlated with promoter methylation (Figures 3F and 3G). Genes correlating with resistance included components of the alternative NF-κB pathway (*TNFRSF13B/TACI* and *MAP3K14/NIK*).

The core NK cell response signature and MHC-I expression correlated with resistance (Figures 3H and 3I), suggesting that pre-existing expression of adaptive response molecules may contribute to cancer cell-intrinsic resistance to NK cells. In addition, several genetic alterations, proteins, miRNAs, and metabolites were associated with sensitivity (Figures 3E and S3C). *TRAF3* and *KRAS* mutations correlated with resistance and *NLRC5* mutations with sensitivity, consistent with the regulation of MHC-I expression by NLRC5[40] (Figure 3E).

CRISPR screens identify genomic determinants of target cell sensitivity and resistance

To investigate underlying mechanisms of cancer cell sensitivity and resistance to NK cells, we performed genome-scale CRISPR loss-of-function (LOF) and gain-of-function (GOF) screens. Pools of transduced tumor cells were co-cultured with expanded NK cells from a minimum of 24 h to up to 2 weeks (Figure 4A; Table S4).

As expected, LOF of MHC-I complex and antigen-presentation machinery genes increased sensitivity across all cell lines, reflecting the "missing-self" mechanism of NK cell activation (Figures 4B, 4C, and S4A). Other sensitizing knockouts (KOs) included genes encoding MHC-I transcriptional regulators (*NLRC5*, *RFXAP*, and *RFXANK*), peptide-loading complex components (*TAP1*, *TAP2*, and *TAPBP*),[41] and IFN-γ pathway components (*JAK1* and *STAT1*).

By contrast, LOF of death receptor pathway genes (*TNFRSF1B*, *TNFRSF10A*, *TNFRSF10B*, *FAS, FADD*, *BID*, and *CASP8*) conferred resistance to NK cell killing, whereas LOF of negative regulators of death receptor signaling (*CFLAR/c-FLIP*, *TRAF2*, and *XIAP*) sensitized multiple cell lines to NK cells (Figures 4B and 4C). Integration of CRISPR screens of NALM6 cells treated with NK or CAR T cells[18] showed shared resistance mechanisms, including *FADD* and *TNFRSF10B*, suggesting death receptor signaling mediating both NK and T cell cytotoxicity (Figure S4B). Gene set enrichment analysis (GSEA) revealed in multiple cell lines enrichment of hits from CRISPR screens for pathways, including FASL/CD95L, transcription of death receptors and ligands, TRAIL, TNFR1-induced NF-κB, IFN-γ, antigen processing and presentation, and class I HLA assembly and peptide loading, supporting the broad relevance of death receptor-mediated apoptosis and MHC-I in regulating NK cell cytotoxicity (Table S4).

Overexpression of several activating NK cell receptor ligands (CD2 ligand *CD58*, NKG2D ligands ULBP1-3 and *MICA*, 2B4 ligand *CD48*, DNAM-1 ligand *PVR*, and 4-1BB ligand *TNFSF9*) sensitized MM1.S cells to NK cells. However, LOF screens revealed a heterogeneous pattern across cell lines. NKp30 ligand *NCR3LG1* played a key role in NK cell cytotoxicity against K562 and MOLM14 cells (Figures 4B and 4C) and was highly expressed in NK-sensitive myeloid leukemias (Figure 3E). Other sensitizing NK cell activating ligands included *CD58* in K562, *CD48* in B-ALL NALM6 and myeloma MM1.S, and *ULBP2* in NALM6 (Figures 4B and 4C). Additionally, several adhesion molecules regulated response to NK cells: the LFA-1 ligand *ICAM1* promoted NK cell killing, whereas adhesion-related glycoproteins *SPN* (*CD43*), the P-selectin ligand *SELPLG* (*PSGL-1*), and *CD44* promoted resistance. PSGL-1, identified in MM1.S, requires O-glycan fucosylation for functionality.[42] Interestingly, depletion of the core fucosylation genes (*FUT8, GMDS*, and *SLC35C1*)[43] sensitized LP1 cells to NK cells, whereas overexpression of the terminal-fucosylation gene *FUT4* induced resistance (Figure S4A). Overexpression of the mucin genes *MUC1* and *MUC21* conferred resistance to NK cells in MM lines. Other genes not previously linked to NK cell cytotoxicity included the peptidase, glycosylation regulator,[44]

Figure 3. PRISM screen of NK cell sensitivity across blood cancer cell lines

(A) PRISM screen workflow.

(B) Examples of NK cell sensitivity dose-response curves. Colored dots represent replicates (n = 8), black dots indicate mean (±SD), and the area under the dose-response curve (AUC), as a quantitative measure of tumor cell survival after NK cell attack, is shown next to the curve.

(C) Boxplot (displayed as in Figure 1E) of sensitivity of different hematological malignancies to NK cell cytotoxicity as AUC of the dose-response curve.

(D) Scatter plot of NK cell activation versus PRISM AUC of the cell lines to NK cells.

(E) Heatmap of molecular correlates of sensitivity to NK cells across blood cancer cell lines. Correlation of expression with methylation is shown on the right, with a separate column indicating significance of the correlation at 5% FDR.

(F–I) Scatter plots of PRISM AUC of cell lines to NK cells versus transcript levels for *NCR3LG1* (F), *ULBP1* (G), baseline expression of core NK cell response gene set (gene set variation analysis [GSVA score]) (H), or HLA I score (I).

Correlation coefficients and p values are obtained using Spearman's rank correlation.

See also Figure S3 and Table S3.

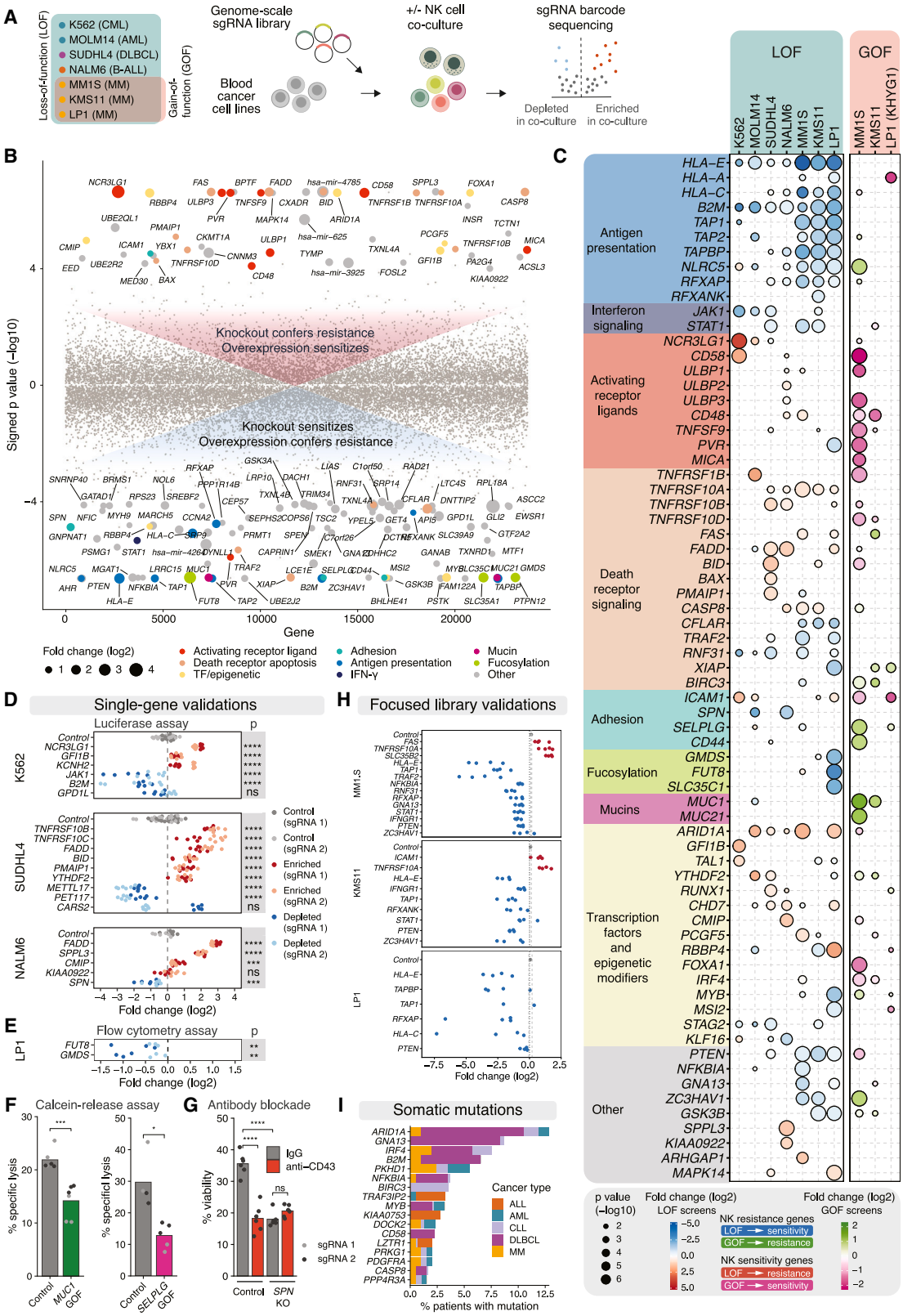

Figure 4. Genome-scale CRISPR screens of NK cell resistance and sensitivity in hematological malignancies

(A) Genome-scale CRISPR screen workflow.

(B) Scatter plot of gene perturbations conferring resistance or sensitivity to NK cells in genome-scale CRISPR screens.

(legend continued on next page)

and positive regulator of MHC-I presentation *SPPL3*,[45] whose LOF in NALM6 induced resistance.

A broad collection of transcriptional regulators and chromatin modifiers regulated NK cell response. Loss of *ARID1A*, a member of the SWI/SNF chromatin remodeling complex, conferred resistance to NK cells (Figure 4B). MM1.S, specifically, became less responsive with *ARID1A* loss and more sensitive with its overexpression. Other gene expression regulators impacting NK responses included erythroid TFs *GFI1B* and *TAL1* in K562 CML cells and the m^6A RNA methylation modifier *YTHDF2* and c-MAF inducing protein (*CMIP*), *FOXA1*, *PCGF5*, *RBBP4*, *IRF4*, *MYB*, and *MSI2* in other cell lines. Additional hits included the NF-κB negative regulator *NFKBIA*, the G-protein alpha subunit *GNA13*, and the antiviral gene *ZC3HAV1*.

We validated results from the genome-scale screens by targeting individual genes (Figures 4D–4G and S4C) and utilizing a focused sgRNA library (Figures 4H and S4D). By targeting individual genes, 85% (17/20) of hits were validated with NK-target cell luciferase assay (Figures 4D and S4C). A flow cytometry-based cytotoxicity assay confirmed that LOF of *FUT8* and *GMDS* sensitized LP1 cells to NK cells (Figure 4E) and reduced surface fucosylation (Figure S4E), an effect phenocopied by the fucosylation inhibitor 2-fluoro-L-fucose[46,47] (Figure S4F). Overexpression of the surface proteins MUC1 and SELPLG in MM1.S cells reduced the NK cell-mediated lysis (Figures 4F and S4C). Furthermore, neutralizing antibody against CD43 (*SPN*) conferred sensitization to NK cells for WT but not *SPN* (CD43) KO NALM6 cells (Figures 4G and S4G), supporting a role for therapeutic targeting of CD43 to enhance NK cell immunotherapy.

Genomic alterations and transcriptional regulation of NK cell susceptibility genes in patient samples

To explore whether CRISPR screen hits are altered in patient samples, we first searched for somatic mutations in public datasets of blood cancers.[36] Somatic mutations occurred in the MHC-I complex subunit gene *B2M*, NF-κB signaling genes (*NFKBIA* and *BIRC3*), TFs and epigenetic modifiers (*ARID1A*, *IRF4*, *STAG2*, and *MYB*), the CD2 ligand *CD58*, the extrinsic apoptosis mediator *CASP8*, and other genes such as *GNA13* (Figures 4I and S5A; Table S5). Many of these mutations were particularly prevalent in DLBCL, and a substantial fraction were stop-gain or frameshift variants leading to LOF (Figures 4I and S5A).

We also investigated DNA copy-number alterations (CNAs) and DNA methylation using multi-omics datasets[35,36] (Figures S5B–S5D). Losses or deletions of *TRAF2* (MM) and *JAK1*, *CD58*, and *ARID1A* (DLBCL) were associated with reduced expression of the respective genes (Figure S5C). CRISPR screen hits, whose expression negatively correlated with DNA methylation of the transcription start site, included *TNFRSF1B*, *ULBP1*, and *ULBP3* (TCGA AML) and *TNFRSF1B*, *ULBP1*, and *PVR* (TCGA DLBCL) (Figure S5D). AML patients with monocytic or myelomonocytic leukemia had the highest *TNFRSF1B* expression, providing examples of how DNA methylation and cell-type-specific transcriptional regulation can influence expression of NK cell susceptibility genes (Figure S5D).

Across all CCLE lines, the NK cell sensitivity regulators *CD48*, *SPN*, *RHOH*, *MYB*, *SELPLG*, and *TNFRSF1B* were selectively expressed in blood cancers (Figure S5E) and highly methylated in solid tumor cell lines, indicating strong lineage-specific regulation of expression (Figure S5E). Conversely, the DNAM-1/CD226 and TIGIT ligand *PVR* and the NKG2D ligand *ULBP3* were enriched in solid tumors, although myeloid malignancies expressed *PVR,* and T cell lymphomas (TCL) expressed *ULBP3* (Figure S5E). These expression patterns were consistent in TCGA patient samples (Figure S5E) and in normal healthy tissues (Figure S5F), indicating cell type, rather than oncogenic transformation, as a key driver of the observed differences. Given their inhibitory function on NK cell cytotoxicity, genes such as *SELPLG*, *SPN*, and *MYB* represent blood-cancer-specific NK cell regulators that present potential therapeutic targets.

The expression of several NK cell evasion genes was associated with inferior survival, such as *MUC1*, *MYB*, *SELPLG*, and *CD44* in MM, and *FUT8* in DLBCL (Figure S5G). By contrast, MHC-I genes (*B2M*, *HLA-C*, and *HLA-E*) were associated with better survival, perhaps reflecting their association with tumor cell responses to cytotoxic T cells. The prognostic effect of several genes varied between cancer types, such as *CD58*, which was associated with better survival in DLBCL but poor prognosis in MM.

Integration of CRISPR and PRISM screens reveals cancer subtype-specific NK cell evasion mechanisms

To explore if mechanisms identified in our CRISPR screens could explain differential NK cell sensitivity across larger cell line panels, we correlated transcript levels (CCLE) of CRISPR screen hits with the PRISM AUC. Across hematologic cancers, high expression of *NCR3LG1*, *ULBP1*, and *PVR* correlated with sensitivity, whereas *B2M*, *NLRC5*, *TAP1*, *CD44*, and *MSI2* correlated

(C) Dot plot of gene perturbations conferring resistance or sensitivity to NK cells in genome-scale CRISPR screens. Shown are selected genes out of those with $p < 0.0001$ in at least one screen or genes validated in separate assays.
(D) Luciferase cytotoxicity assays for validation of individual hits of genome-wide screen hits with six replicates (dots) per single guide RNA (sgRNA); two sgRNAs per gene.
(E) Flow cytometry validation of core fucosylation gene knockout effect on sensitivity to NK cells in MM cell line LP1 as $\log_2$FC of relative cell counts of knockout to control cells with three replicates (dots) per sgRNA; 2 sgRNAs per gene.
(F) Calcein AM release assay in MM1.S MM cells overexpressing either *MUC1* or *SELPLG* versus control sgRNAs. Data are from a single donor (NK2) at an effector-to-target ratio of 3:1 (*MUC1*) or 1:1 (*SELPLG*). Dots indicate three replicates for each of the two sgRNAs, bar height indicates the mean.
(G) Effect of antibody-mediated CD43 (SPN) blockade on NK cell cytotoxicity (donor NK1) in control and *SPN* knockout NALM6 cell lines. Bar heights depict the mean percentage of viable NALM6 target cells measured by luciferase assay and dots represent three replicates per sgRNAs (n = 2). Data are normalized to non-NK-treated target cells (100% viability).
(H) Selected genes validated using pooled CRISPR screens with focused libraries targeting genome-wide screen hits in MM cell lines. Olfactory receptor (OR) genes were used as controls, in gray is the average of all OR gene sgRNA $\log_2$FC values, and the dashed lines represent the 95% confidence interval.
(I) Frequency of mutations in CRISPR screen hit genes in patients with hematological malignancies. Only genes with mutations in >1.5% patients cumulatively in all cancer types are shown.
See also Figures S4 and S5 and Tables S4 and S5.

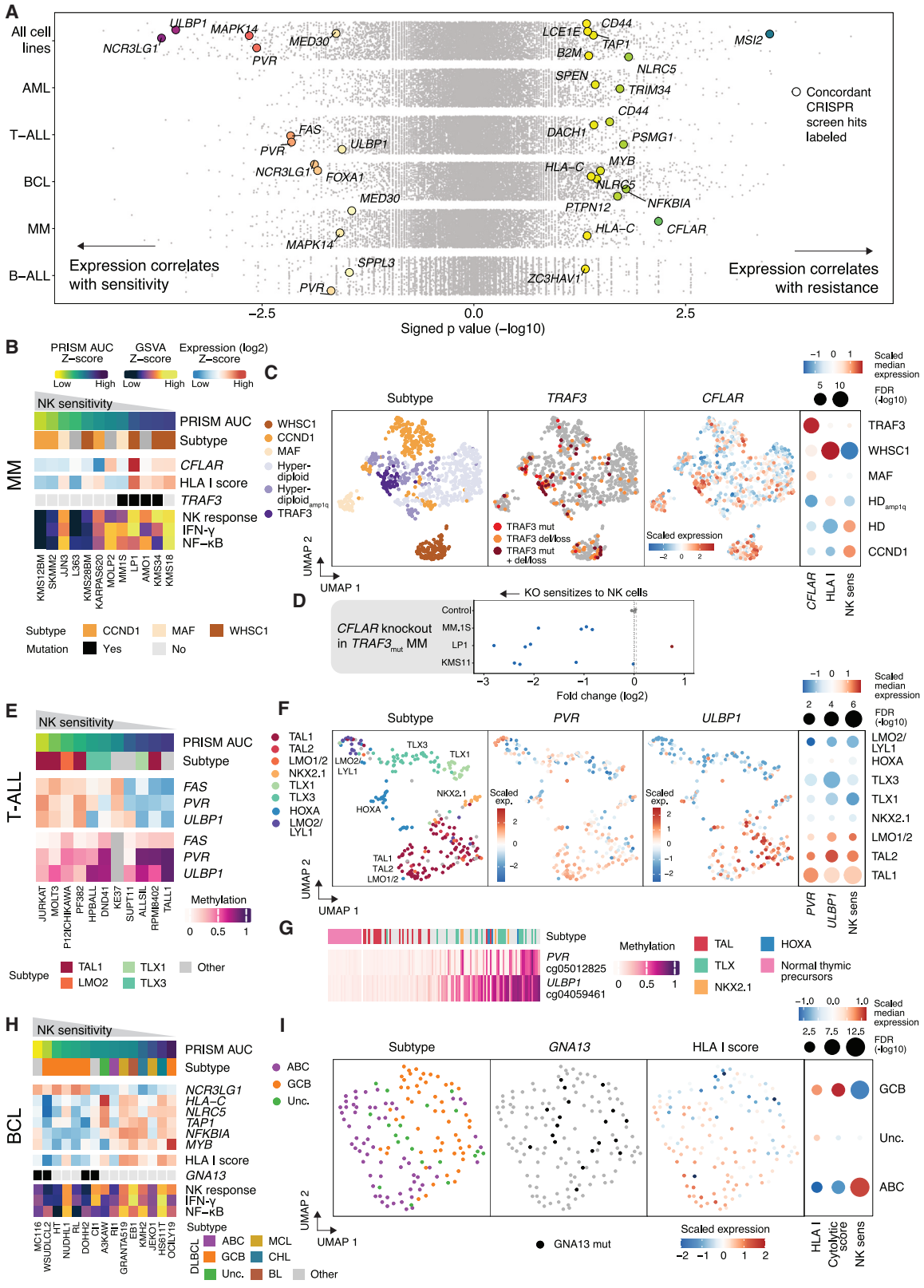

(legend on next page)

with resistance (Figure 5A; Table S6). The IFN-γ response signature, TNF signaling via NF-κB, the core NK cell response signature, and HLA I score correlated with resistance in MM and BCL and IFN-γ response additionally in AML (Figures S5H and S5I).

In MM, NK cell resistance correlated with expression of *CFLAR* encoding c-FLIP, a suppressor of death receptor-mediated apoptosis, MHC-I genes, the t(4;14) (WHSC1) translocation, and inactivating mutations in *TRAF3* (which cause activation of non-canonical NF-κB signaling[48,49]) (Figures 5A and 5B). As *CFLAR* is a known NF-κB target gene,[50] *TRAF3* mutations could confer NK cell resistance by inducing *CFLAR*, resulting in impaired death receptor-mediated apoptosis. We developed an NK cell sensitivity signature comprising genes whose expression correlated with sensitivity in the cell lines and applied this signature to identify patient subgroups with molecular profiles matching NK-sensitive versus NK-resistant lines. In MM, this sensitivity signature was low in the WHSC1 subgroup (Figure 5C), indicating that the cell lines recapitulate molecular subtypes found in MM patients. *CFLAR* expression was enriched in patients with *TRAF3* alterations and MHC-I expression in the WHSC1 subgroup, consistent with the cell line data (Figure 5C). Finally, LOF of *CFLAR* induced increased response to NK cells in *TRAF3*-mutant MM1.S, KMS11, and LP1 cells (Figure 5D). These results indicate that *TRAF3* and *WHSC1* alterations contribute to NK cell evasion in MM.

In T-ALL, NK cell sensitivity correlated with expression of the death receptor *FAS*, the DNAM-1 ligand *PVR*, the NKG2D ligand *ULBP1*, and the TAL1 and LMO2 genetic subtypes representing late cortical differentiation[51] (Figures 5A and 5E). By contrast, other T-ALL lines showed low expression and high DNA methylation of *PVR* and *ULBP1*. Consistently, in T-ALL patients,[52] *PVR* and *ULBP1* expression was enriched in the TAL1, TAL2, and LMO2 genetic subtypes corresponding to the late cortical stage, in contrast to other subtypes including the early cortical stage TLX1 and TLX3, and the more immature stage LMO2/LYL1 (Figure 5F). *PVR* and *ULBP1* were unmethylated in patients with the TAL subtype and healthy T cells at all maturation stages[53] but showed increased methylation in other subtypes. Therefore, epigenetic control may underlie the cancer-specific silencing of *PVR* and *ULBP1* in immature and early cortical T-ALL (Figure 5G).

Among BCL lines, the germinal center B (GCB) cell subtype tended to be more NK cell sensitive compared with other subtypes, including MCL, CHL, Burkitt lymphoma (BL), and activated B cell (ABC) (Figure 5H). Expression of several CRISPR hits correlated with sensitivity (e.g., *NCR3LG1*) or resistance (e.g., *NLRC5*, *TAP1*, *NFKBIA*, *MYB*, *IRF4*, and MHC-I), also consistent with the IFN-γ and NF-κB response gene sets being enriched in NK-resistant BCL lines. Mutations in *GNA13* correlated with NK cell sensitivity, in line with our CRISPR screen data (Figures 4C and 4H). In DLBCL patients, the PRISM-derived NK cell sensitivity signature was consistently enriched in the GCB subtype, which harbored *GNA13* mutations and showed decreased expression of *NLRC5*, MHC-I genes, *TAP1*, *NFKBIA*, and *MYB* compared with ABC tumors (Figure 5I).

Single-cell transcriptomics CRISPR screens reveal NK cell evasion mechanisms

We used CRISPR screens with a single-cell transcriptome readout (CRISPR droplet sequencing [CROP-seq])[54] to reveal mechanisms whereby selected genes impact sensitivity to NK cells, focusing on highly scoring hits from the genome-scale screens (Figure 6A). From six single-cell screens, we obtained a total of 118,968 cells with an assigned sgRNA, with three sgRNAs targeting each of the 65 perturbed genes and, on average, 128 cells representing each sgRNA (Table S7).

We analyzed differentially expressed genes (DEGs) between malignant cells harboring each perturbation and those carrying control sgRNAs, both with and without NK cell exposure. Out of the 65 perturbed genes, 30 showed no substantial transcriptomic changes (<5 DEGs, Figures 6B and S6A). These included the cell-surface protein genes *NCR3LG1*, *CD58*, *ICAM1*, *HLA-E*, *SPN*, *SELPLG*, and *MUC1*, suggesting that their physical interaction with NK cell surface molecules is the main mechanism mediating their effect on NK cell cytotoxicity. For the 35 perturbations with a transcriptomic phenotype, we examined the common and distinct patterns by comparing the overlap of the DEGs (Figures S6B and S6C) and by using uniform manifold approximation and projection (UMAP) dimensionality reduction after performing linear discriminant analysis[55] (Figures 6C

Figure 5. Integration of CRISPR and PRISM screens reveals cancer subtype-specific NK cell evasion mechanisms

(A) Gene expression correlations with PRISM AUC after exposure to NK cells shown as signed p values of the Spearman's rank correlations using CCLE data. CRISPR screen hit genes ($p < 0.0001$) showing a correlation with PRISM AUC ($p < 0.05$) to the same direction are colored and labeled. Dot color indicates the signed p value.

(B) Heatmap of MM cell lines ordered by sensitivity to NK cells showing genetic subtypes, *CFLAR* expression, HLA I score, *TRAF3* mutation status, and GSVA scores of the core NK cell response, hallmark IFN-γ response and hallmark TNFA signaling via NF-κB gene sets.

(C) UMAPs of MM transcriptomic data from CoMMpass (n = 767). Dot plot on the right shows the median expression of *CFLAR*, HLA I score, and NK sensitivity signature (50 genes most significantly correlated with PRISM AUC) across CoMMpass subtypes. Dot size indicates significance of differential expression between the indicated subtype and all other subtypes.

(D) Effect of *CFLAR* knockout in genome-wide CRISPR screens in *TRAF3*-mutated MM cell lines. Olfactory receptor (OR) genes were used as a control; in gray is the average of all OR gene sgRNA $\log_2$FC values, the dashed lines represent the 95% confidence interval.

(E) Heatmap of T-ALL cell lines ordered by PRISM AUC after NK cell treatment showing genetic subtypes, *FAS, PVR*, and *ULBP1* expression and methylation.

(F) UMAPs of T-ALL transcriptomic data from Liu et al. (n = 262). Dot plot on the right shows the median expressions of *PVR*, *ULBP1*, and NK sensitivity signature across T-ALL subtypes. Dot size as in (C).

(G) Heatmap of *PVR* and *ULBP1* methylation in T-ALL patients (n = 109) and healthy controls (n = 20) from Roels et al. (GSE155333). Healthy thymocytes are shown on the left. Genetic subtypes according to Roels et al. are shown above.

(H) Heatmap of B cell lymphoma (BCL) cell lines ordered by sensitivity to NK cells showing lymphoma subtypes, expression of CRISPR hits correlating with PRISM AUC, HLA I score, *GNA13* mutations, and GSVA scores of the same gene sets as in Figure 5B.

(I) UMAPs of DLBCL transcriptomic data from Chapuy et al. (n = 137). Cell-of-origin subtypes, *GNA13* mutations, and HLA I score are colored on the plots. Dot plot on the right shows the median HLA I score, cytolytic score, and NK sensitivity signature across DLBCL subtypes. Dot size as in (C).

See also Table S6.

CellPress
OPEN ACCESS

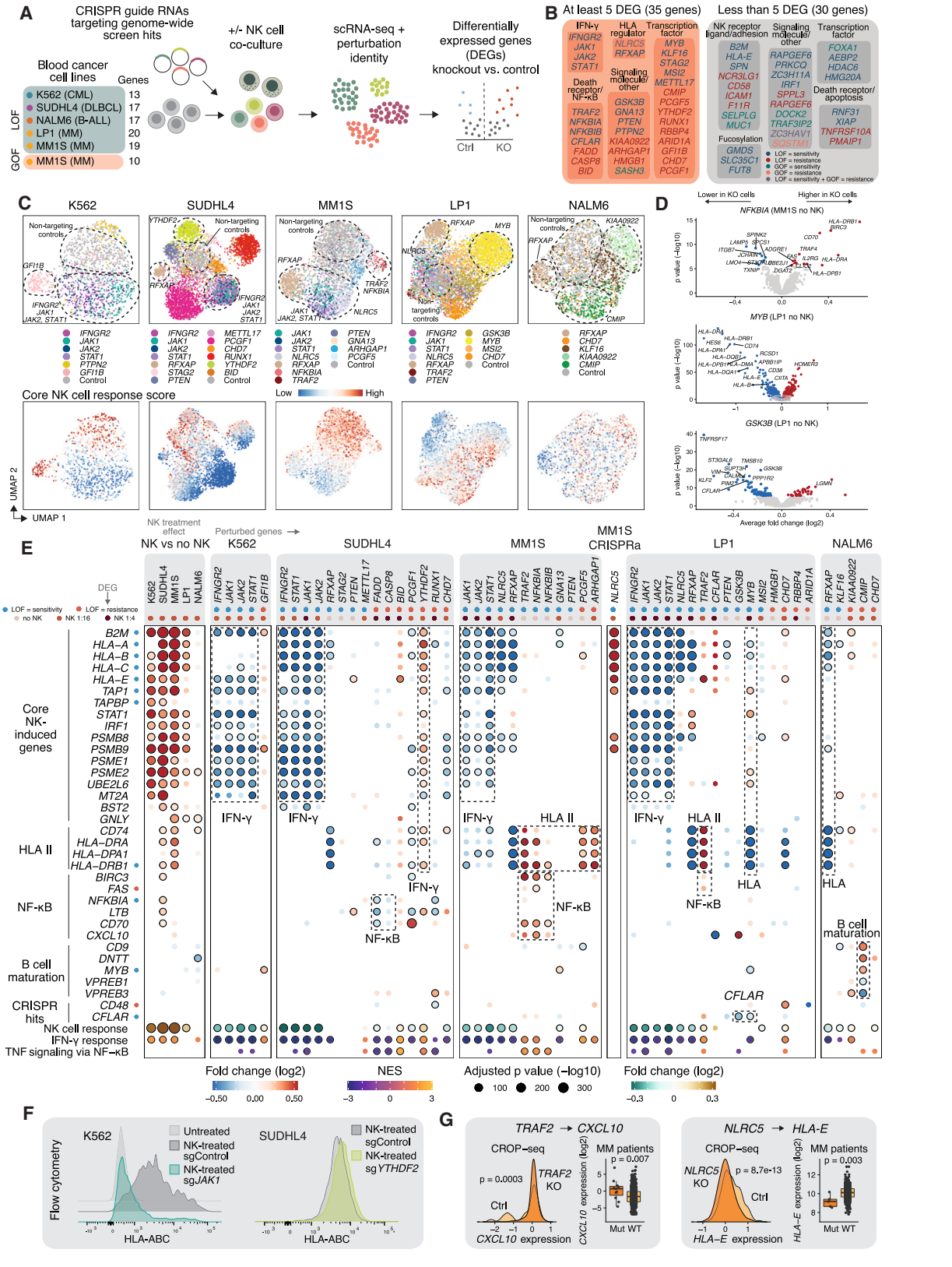

(legend on next page)

and S6D). Perturbations targeting IFN-γ signaling mediators (*IFNGR2*, *JAK1*, *JAK2*, and *STAT1*) grouped together in the UMAP reduced space, as did those targeting NF-κB regulators (*TRAF2*, *NFKBIA*, and *NFKBIB*), consistent with common transcriptional changes induced by perturbing genes of the same pathway. By contrast, most other perturbations grouped individually, indicating distinct transcriptomic phenotypes. Perturbations targeting IFN-γ and death receptor signaling mediators induced substantial transcriptomic changes only in the presence of NK cells (Figures S6A and S6E). Several perturbations influenced the core NK cell response reflecting MHC-I genes and IFN-γ signaling (Figures 6C and 6E), suggesting that these genes may regulate sensitivity to NK cells by influencing the transcriptomic response to NK cell attack.

We hypothesized that perturbing a CRISPR screen hit might affect the expression of other hits, revealing functional connections between them. Indeed, LOF of genes encoding IFN-γ signaling mediators (*IFNGR2*, *JAK1*, *JAK2*, and *STAT1*) prevented the NK cell-driven induction of the MHC-I complex transcript (Figures 6C, 6E, S6C–S6E, and S7A) and protein levels (Figure 6F). Whereas LOF of the IFN-γ signaling mediators showed a phenotype only in the presence of NK cells (Figures S6A–S7C), silencing of the HLA gene transactivator complex components *NLRC5* and *RFXAP* downregulated MHC-I genes both with and without NK cell exposure (Figure S7B).

Several genes that promoted NK cell killing, including *GFI1B* in K562, *YTHDF2* and *BID* in SUDHL4, *PCGF5* in MM1.S, and *KIAA0922* in NALM6, emerged as negative regulators of IFN-γ signaling and MHC-I expression (Figures 6C, 6E, 6F, and S6C). Conversely, LOF of *MYB* in LP1 cells reduced both MHC-I and MHC-II expression, indicating MYB as a positive regulator of antigen-presentation genes (Figures 6C–6E and S7B). DEGs between KO and control cells were mostly concordant at different time points tested in MM1.S cells (Figure S6D). However, disruption of IFN-γ-JAK-STAT signaling had more pronounced effects at the earlier 3 and 6 h time points and effects on MHC-I expression were evident only at 24 h, consistent with the previously observed temporal pattern of MHC-I induction (Figure 2E).

We integrated our CRISPR data with those on MHC-I regulators by Dersh et al.[56] (Figure S7D). LOF of *ARID1A*, a negative regulator of MHC-I in the BJAB cell line,[56] concordantly conferred resistance to NK cells in four of our genome-scale screens. By contrast, KO of *TRAF2* and *CFLAR*, also negative regulators of MHC-I in Dersh et al. sensitized MM cells to NK cells in our screens, suggesting alternate, disease-specific mechanisms overriding the potential MHC-I modulation.

Among potential mechanisms distinct from MHC-I regulation, disruption of *NFKBIA* and *TRAF2* in MM1.S caused increased expression of the death receptor *FAS*, which promoted NK cell susceptibility in the MM1.S CRISPR screen (Figures 6D, 6E, and S7B). *GSK3B* and *MYB* LOF in LP1 downregulated *CFLAR*, a negative regulator of death receptor signaling and NK cell resistance gene identified in the CRISPR screens (Figures 6D, 6E, and S7B). *CMIP* disruption in NALM6 downregulated *CD48*, which is a ligand for the activating receptor 2B4 and promotes NK cell responsiveness of NALM6 cells (Figures 6E and S7B).

Our CROP-seq studies also identified other perturbation-induced transcriptional events, not necessarily involving CRISPR screen hits, which could influence tumor-NK cell interactions. In SUDHL4 cells, LOF of the death receptor apoptosis mediators *FADD* or *CASP8* inhibited the NK cell-induced NF-κB activation (Figures 6E and S7C). In addition to mediating apoptotic signals, FADD and CASP8 thus appear to regulate the transcriptomic response to NK cell attack.[57,58] By contrast, silencing of *TRAF2*, *NFKBIA*, or *NFKBIB* in MM1.S cells induced known NF-κB targets (Figures 6D, 6E, and S7A), such as *BIRC3* and *CD70*, and the chemokines *CXCL10* and *CCL5*,[59,60] which may further increase T and NK cell recruitment.[61–64] Silencing of *CMIP* in the pre-B-ALL cell line NALM6 led to increased expression of *DNTT* (*TdT*) and *CD9*, markers of early pro-B cells, and concomitant downregulation of genes expressed in more differentiated pro-B cells, including *CD79A*, *VPREB1*, and *VPREB3* (Figures 6E, S6D, and S7A). A more immature B cell state repressed by *CMIP* may therefore drive resistance to NK cell killing.

Next, we asked whether mutations in NK cell susceptibility genes in patient tumor cells are associated with transcriptomic alterations similar to those observed by CROP-seq. We compared the DEGs of each perturbation in CROP-seq with DEGs between patients with and without mutations in the same gene (Figures 6G and S7E). MM patients with mutations in the NF-κB negative regulators *TRAF2* and *NFKBIA* expressed higher levels of NF-κB target genes also identified experimentally by CROP-seq (Figures 6G and S7E). Moreover, MM patients with *NLRC5* mutations had lower *HLA-E* expression consistent with CROP-seq data (Figures 6G and S7E), indicating that although rare, *NLRC5* mutations in MM may result in an NK-sensitive phenotype (Figure 6G).

Cancer-cell intrinsic perturbations modulate NK cell transcriptomic states

We examined whether perturbing CRISPR screen hits in cancer cells could influence the NK cell activation states (Figure 7A). To

Figure 6. Single-cell transcriptomics CRISPR screens of cancer cell-intrinsic NK cell sensitivity regulators

(A) Single-cell CRISPR screening (CROP-seq) workflow.

(B) Genes targeted in CROP-seq experiments, divided into groups with at least or less than five differentially expressed genes (DEGs) compared with non-targeting control cells in any of the conditions (no NK, NK 1:16, or NK 1:4), after 24 h co-culture.

(C) UMAPs of CROP-seq data after linear discriminant analysis in the indicated cell lines at 1:16 effector-to-target ratio.

(D) Volcano plots of differentially expressed genes with selected perturbations versus control sgRNA-expressing cells.

(E) Dot plot of genes differentially expressed in cancer cells (rows) where the indicated genes (columns) are perturbed compared with cells expressing control sgRNAs. Perturbed genes with at least 5 DEGs are shown. Only dots where $p < 0.05$ are shown, circled dots indicate adjusted $p < 0.05$. Selected molecular processes regulated by the perturbed genes are highlighted using dotted lines.

(F) Flow cytometry histograms of effects of *JAK1* and *YTHDF2* disruption on HLA-ABC surface expression.

(G) Examples of transcriptional changes induced by CROP-seq perturbations with consistent changes in MM patients (CoMMpass) harboring mutations in the same genes. Perturbed cells are in dark yellow, controls in light yellow. Boxplots displayed as in Figure 1E; dots indicate individual patient samples.

See also Figures S6 and S7 and Table S7.

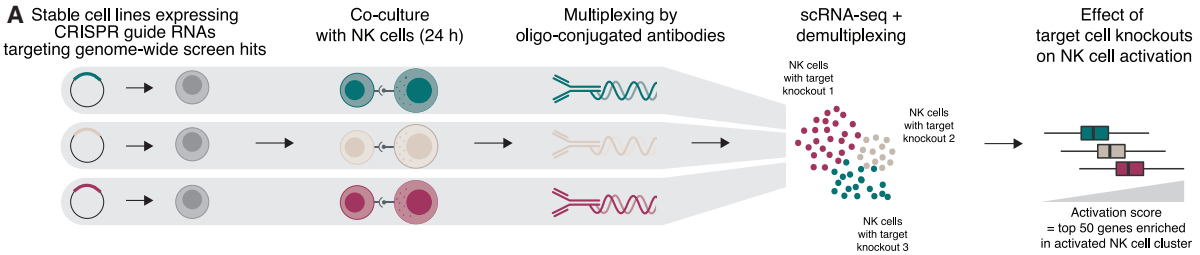

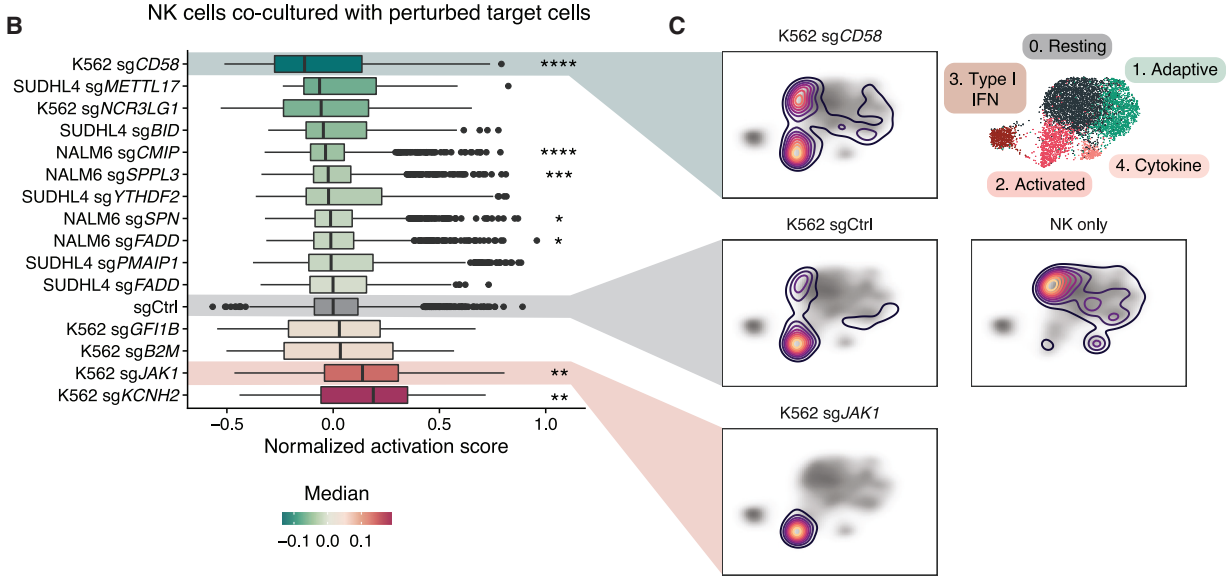

D

Perturbations sensitizing to NK cell cytotoxicity

Pathway/ group	Gene	Proposed mechanism of KO based on RNA-seq	Other effects of KO
IFN-γ signaling	*IFNGR2* *JAK1* *JAK2* *STAT1*	*B2M* ↓ *HLA-A/B/C/E* ↓ NK activation ↑	*MHC-II* ↓
MHC regulators	*NLRC5*	*B2M* ↓ *HLA-A/B/C/E* ↓	
	RFXAP	*B2M* ↓ *HLA-A/B/C/E* ↓	*MHC-II* ↓ *BTN2A2* ↓ *BTN3A2* ↑
NF-κB signaling	*NFKBIA* *NFKBIB* *TRAF2*	*FAS* ↑	*CXCL10* ↑ *CD70* ↑ *MHC-II* ↑
Transcription factors/ signaling	*MYB*	*B2M* ↓ *HLA-A/B/C/E* ↓	*MHC-II* ↓
	GSK3B	*CFLAR* ↓	

Perturbations conferring resistance to NK cell cytotoxicity

Pathway/ group	Gene	Proposed mechanism of KO based on RNA-seq	Other effects of KO
Death receptor signaling	*FADD* *CASP8*	Apoptosis resistance	*NF-κB* ↓
Transcriptional regulators	*YTHDF2*	*B2M* ↑ *HLA-A/B/C/E* ↑	IFN-γ response ↑ *MHC-II* ↑
	PCGF5	*HLA-B* ↑	*MHC-II* ↑
	GFI1B	*B2M* ↑ *HLA-C/E* ↑	
	KIAA0922	*B2M* ↑ *HLA-B* ↑	
	CMIP	*CD48* ↓ NK activation ↓	B cell maturation ↓
Activating ligands	*CD58*	NK activation ↓	

(legend on next page)

quantify the effects of the target cell KOs on NK cell activation, we computed an activation score for each NK cell, comprising 50 genes most significantly enriched in the activated NK cell state (Figure 7B), and mapped the NK cells from the present experiment to the UMAP dimensionality reduction from the original co-culture experiment (Figure 7C). Resistance-inducing perturbations (e.g., LOF of *CD58* in K562 cells or of *CMIP* and *SPPL3* in NALM6 cells) decreased NK cell activation scores (compared with non-targeting control sgRNAs in respective lines) (Figure 7B) and prevented NK cell transition from resting to activated state (Figure 7C). By contrast, *JAK1* LOF induced stronger NK cell activation, consistent with its sensitizing effect (Figures 7B and 7C). Collectively, the perturbation-induced transcriptional changes both in NK and target cells offer plausible mechanisms for how the genes identified in CRISPR screens control sensitivity to NK cells and provide a comprehensive resource of other immunoregulatory effects (Figure 7D).

DISCUSSION

In this study, we comprehensively examined the molecular changes induced by the interaction of NK cells with malignant hematopoietic target cells at single-cell resolution, assessed cancer-type sensitivities to NK cells by PRISM profiling, and identified genes and pathways affecting NK cell susceptibility via CRISPR screens. A key finding is the diversity of mechanisms influencing NK cell susceptibility across different cancers, highlighting the importance of considering cancer subtypes and genetics for personalized NK cell-based therapies.

The diverse adaptive, interaction-induced responses reflected the heterogeneity, with different tumor cell lines causing NK cells to transition to various activated states ranging from significant shifts to minimal changes. The NK cell states emerged both in expanded and unexpanded PBMC-derived NK cells upon tumor cell exposure. The activated state included genes encoding receptors, such as 4-1BB, OX-40, and CRTAM, which are induced by NK cell activation.[65–67] The IFN-I state resembles IFN-I-responding cells[9] and inflamed NK cells,[10] enriched in IFN-I-high inflammatory conditions, such as severe COVID-19 infection.[68,69] The cytokine state has been described before in non-expanded NK cells and sometimes referred to as active NK cells.[10,69] Given its low presence in unchallenged NK cells, this stage may signify cells primed for response but not yet fully activated because the subsequent activated states are absent in unchallenged NK cells. As the tumor-induced states correlated with increased cytotoxicity against target cells, interventions promoting the activated state, such as agonistic antibodies for activating immune checkpoint receptors, could improve NK cell immunotherapies. Some of the receptors induced in the activated (TIM-3, TIGIT, and possibly also 4-1BB[65] and GITR[70]) and IFN-I (LAG3) states inhibit NK cell function, and blocking these could further augment the function of NK cells.

The gene signature recurrently induced in cancer cells in response to NK cell exposure, reflecting IFN-γ signaling and MHC-I, is consistent with a negative feedback loop suggested in early studies.[71,72] Our single-cell CRISPR data confirm the role of IFN-γ signaling through JAK-STAT. When NK cells lack inhibitory KIRs (e.g., in the NK-92 cell line[73]), their activity against target tumor cells (e.g., the K562 line) may not be enhanced by loss of IFN-γ signaling,[74] consistent with this effect being mediated by KIR-MHC interactions. The IFN-I signature induced in a subset of cell lines may reflect the IFN-stimulated resistance signature described previously to mediate immunotherapy resistance.[75,76]

The same transcriptomic signature that was induced in cancer cells upon NK cell attack correlated with resistance to NK cells across blood cancer cell lines. Pre-existing activation of adaptive resistance pathways may therefore explain primary resistance of cancer cells to NK cells. Conversely, as defects in IFN signaling and antigen presentation cause resistance to T cells,[77,78] NK cells could offer an effective and individualized alternative. In addition, because *JAK1* KO in myeloid leukemia cells strongly potentiated the NK activation signature, pharmacological inhibition of the JAK-STAT pathway is an interesting treatment option for future combination therapies with NK cells.

Our findings challenge the notion that expression of activating ligands for NK cells is a general feature of transformed cells (“altered-self”). Instead, the cancer type, lineage, and genomics appear to jointly define the expression patterns. Key activating ligands, including *NCR3LG1*, *PVR*, and *ULBP1*, were highly expressed in myeloid as opposed to lymphoid leukemias, consistent with AML being sensitive compared with pre-B-ALL as previously suggested.[79] Furthermore, *NCR3LG1*, identified also in previous CRISPR screens in the myeloid K562 cells and colorectal cancer lines[21,74] promoted NK cell cytotoxicity in myeloid leukemias but not lymphoid cancers. Consistently, an immature phenotype less differentiated toward the myeloid lineage may enable evasion from NK cells in AML.[80,81] As genes encoding activating ligands, such as *PVR*, or apoptotic mediators, such as *TNFRSF1B*, were highly expressed also in the normal counterparts of myeloid malignancies, the observed expression pattern may originate from normal hematopoietic differentiation rather than being a feature acquired upon transformation.

In addition, our findings implicate genomic subtypes of blood cancers with NK cell evasion. In T-ALL, the activating ligands *PVR* and *ULBP1* exhibited low expression in the less differentiated NK-resistant TLX-driven subtypes. *CFLAR* expression driving NK resistance in *TRAF3*-altered MM and high MHC-I expression in the WHSC1 subtype represent further examples

Figure 7. Effects of cancer cell perturbations on NK cell activation states

(A) Workflow of identification of NK cell responses to cancer cells carrying different perturbations using single-cell transcriptomics.

(B) Boxplot of NK cell activation scores (top 50 genes enriched in the activated state) in single NK cells across different target cell perturbations. p values between each perturbation and the cell line-specific control are obtained using Wilcoxon rank sum test with Benjamini-Hochberg adjustment. Boxplots are displayed as in Figure 1E.

(C) UMAPs of NK cells cultured alone or co-cultured with K562 cells expressing the indicated sgRNAs. Contour lines and their color indicate the density of NK cells in different regions of the UMAP reduced space. Gray shading in the background shows the density of all NK cells from Figure 1B. Clusters from Figure 1B are shown on the right for reference.

(D) Summary tables of key findings from single-cell transcriptomics assays on perturbation effects both in the target cells (CROP-seq) and in NK cells.

of NK cell evasion driven by the genetic makeup of the cancer cells. Given that *CFLAR* can influence sensitivity of cancer cells not only to NK cells but also T cells,[19,82] this finding may have relevance to immunotherapy sensitivity beyond NK cells.

Our CRISPR screens also implicated many previously underappreciated gene classes in the regulation of NK cell responses, including mucins, fucosylation/glycosylation regulators, glycoproteins, and a range of transcriptional regulators. The decreased NK cell cytotoxicity caused by *MUC1* overexpression is consistent with a recent report that MUC1 C-terminal transmembrane subunit suppresses NK cell killing via MICA/B repression in mucin-expressing solid tumors.[83] Although our screens in the MM cell lines LP1 identified the core fucosylation genes *FUT8*, *GMDS*, and *SLC35C1*, previous screens in colorectal cancer cell lines identified another glycosylation enzyme, *SLC35A2*, as a driver of resistance to NK cells.[21] The influence of core fucosylation on human IgG1 Fc affinity for the FcγRIII is previously documented, and glycoengineering of monoclonal antibodies to reduce core fucosylation has proven effective in enhancing ADCC (antibody-dependent cellular cytotoxicity).[84,85] The glycosylation regulator SPPL3, heavily glycosylated mucins, and the recently identified Siglec-7 ligands SPN (CD43) and SELPLG (PSGL-1)[86,87] point toward an important role for glycosylation in the interactions of NK cells with cancer cells. The hematopoietic lineage-driven expression of some of these NK cell regulators (*SPN* and *SELPLG*) support that blood cancers may interact with NK cells in a distinct way compared with solid tumors, potentially because they originate from immune cells naturally interacting with NK cells.

Intact death receptor signaling was important for NK cell responsiveness of several cell lines but redundant in others such as K562, highlighting the heterogeneity in apoptotic mechanisms among NK-sensitive tumor lines. The reliance on distinct apoptotic pathways in different cancers may impact approaches to sensitize tumors to NK cells, including BH3 mimetics.[88] As the death receptor pathway can also mediate bystander killing,[89] the differential sensitivity of cancers may influence the efficacy of both NK and T cell immunotherapies.

In summary, our study provides a comprehensive picture of the adaptive molecular changes in interacting NK and blood cancer cells and molecular mechanisms of response and resistance to NK cell cytotoxicity. These molecular profiles offer a resource informing efforts to develop personalized NK cell immunotherapy strategies for hematological malignancies.

Limitations of the study

Our single-cell analyses of interaction-induced cell states, including CROP-seq studies, relied on transcriptomics, warranting cell-surface proteomic studies of these states. Our PRISM and CRISPR studies included 63 and 7 cell lines, respectively, from different blood cancer types, but some more rare blood cancer types were not represented. Because many of the hits in our screens were found only in some cell lines, our data stress the importance of large unbiased screens in diverse cancer types. We anticipate our findings on the heterogeneity between cancer types to stimulate similar efforts in other infrequent malignancies. We envision our findings to encourage more frequent sampling during *in vivo* adoptive cell transfer in patients to capture the changes occurring immediately upon NK-cancer cell interaction.

STAR★METHODS

Detailed methods are provided in the online version of this paper and include the following:

- KEY RESOURCES TABLE
- RESOURCE AVAILABILITY
  - Lead contact
  - Materials availability
  - Data and code availability
- EXPERIMENTAL MODEL AND STUDY PARTICIPANT DETAILS
  - Cell lines
  - Primary NK cell isolation and expansion
- METHOD DETAILS
  - Co-culture assays with multiplexed scRNA-seq readout
  - Cytokine analysis
  - Pooled PRISM screen of NK cell cytotoxicity against DNA-barcoded cancer cell lines
  - Genome-scale CRISPR-Cas9-based gene editing or gene activation screens
  - CRISPR screens with focused sgRNA library
  - Individual gene validations
  - Analysis of CRISPR screen hit mutations and gene expression
  - Multi-omics correlations with PRISM-based NK cell sensitivity
  - Patient genomic data analysis
  - Single-cell transcriptomics CRISPR screens
- QUANTIFICATION AND STATISTICAL ANALYSIS

SUPPLEMENTAL INFORMATION

Supplemental information can be found online at https://doi.org/10.1016/j.immuni.2023.11.008.

ACKNOWLEDGMENTS

We thank Prof. Yenan Bryceson and Drs. Mikko Keränen, Oscar Brück, Mikko Myllymäki, Sofie Lundgren, Leo Meriranta, and Francesca De Lorenzo for insightful comments. We acknowledge the Biomedicum Sequencing Laboratory and Virus Core supported by the Biocentrum Helsinki; the Helsinki Institute of Life Science (HiLIFE), the Biomedicum Helsinki Flow Cytometry Core Unit, and the FIMM Single-Cell Analytics and Sequencing units supported by HiLIFE and Biocenter Finland; the Finnish Red Cross Blood Service biobank; and the Team 11 of the Centre de Recherche en Cancérologie et Immunologie Intégrée de Nantes-Angers (CRCI^{2}NA) led by Dr. Catherine Pellat-Deceunynck for their support and services. The study was supported by grants from the Cancer Foundation Finland, Academy of Finland, Jane and Aatos Erkko Foundation, Sigrid Juselius Foundation, Gyllenberg Foundation, State funding for the University-level Health Research in Finland, and HiLIFE fellow funds (to S.M.), Stand Up To Cancer (SU2C) Convergence 2.0 Grant (S.G., M.S., and C.S.M.), SU2C Phillip A. Sharp Award for Innovation in Collaboration (M.S. and C.S.M.), Leukemia and Lymphoma Society (LLS) Scholar Award (C.S.M.), de Gunzburg Myeloma Research Fund (O. Dashevsky and C.S.M.), International Myeloma Society (IMS) (C.S.M.), Shawna Ashlee Corman Investigatorship in Multiple Myeloma Research (C.S.M.), Cobb Family Myeloma Research Fund (S.G. and C.S.M.), and Ludwig Center at Harvard (C.S.M.). The collaborating laboratories have also been partially supported by grants from the NIH (R01 CA276156 to C.S.M. and S.M., R01 CA196664 to C.S.M., and U01 CA225730 to C.S.M.), the Lauri Strauss Leukemia Foundation (to O. Dashevsky and R.S.), and LLS Translational Research Program (C.S.M.

and S.M.). O. Dufva was supported by grants from the Biomedicum Helsinki Foundation, Finnish Medical Society, Cancer Foundation Finland, K. Albin Johansson Foundation, Emil Aaltonen Foundation, Ida Montin Foundation, Paulo Foundation, Finnish Blood Disease Research Foundation, and Finnish Hematology Association. S.G. was supported by the ASCO Conquer Cancer Young Investigator Award, the IMS-Paula and Rodger Riney Foundation Career Development Award, and the Associazione Italiana per la Ricerca sul Cancro (AIRC, Italian Association for Cancer Research).

AUTHOR CONTRIBUTIONS

O. Dufva and S.G. designed and conducted experiments, analyzed and interpreted data, and wrote the manuscript. J. Huuhtanen contributed to the design and analysis of scRNA-seq experiments. O. Dashevsky and H.D. designed and conducted experiments. K.S. and J.K. performed CRISPR screens and generated CRISPR-Cas9-edited cell lines. P.N., J.B., H. Lähteenmäki, and P.R. conducted experiments and performed NK cell expansions. J.L. and A.N. performed scRNA-seq library preparation, and B.R.G. performed scRNA-seq data preprocessing. T.H. and P.E. performed CRISPR screen sequencing. J.T. and E.L. assisted with computational analysis. J. Härkönen, P.P., and M. Heinäniemi provided assistance with analysis of multi-omic datasets. M. Hollmén performed cytokine analyses. S.Y. assisted with focused library CRISPR screens. R.S. generated dCas9/VP64 cell lines. J.A.R. provided advisory roles and assisted with PRISM screens design. D.A.B. and R.R. provided advisory roles. M.S. assisted with design of initial CRISPR screen on myeloma cells. H. Lähdesmäki provided insights on computational analyses. D.A.L. provided expanded NK cells and assistance with NK cell expansion methods. R.D.M.S. and M.K. designed and performed computational analyses of CRISPR screen data. S.M. and C.S.M. supervised the project, led the design, interpretation, and analysis of experiments, and contributed to the writing and preparation of the manuscript. All co-authors provided feedback and approved the final version of the manuscript.

DECLARATION OF INTERESTS

M.S. and C.S.M. are authors of a patent application related to antitumor activity of NK cells. C.S.M. is a member of the Scientific Advisory Board of Adicet Bio and also discloses consultant honoraria from Fate Therapeutics, Ionis Pharmaceuticals, FIMECS, Secura Bio, and Oncopeptides and research funding from Sanofi, Merck KGaA/EMD Serono, Arch Oncology, Karyopharm, Nurix, Eisai/H3 Biomedicine, Novartis, BMS, Abcuro, and Springworks. S.M. has received honoraria and research funding from Novartis, Pfizer, and Bristol-Myers Squibb and honoraria from Dren-Bio (not related to this study).

INCLUSION AND DIVERSITY

We support inclusive, diverse, and equitable conduct of research.

Received: October 31, 2022
Revised: June 19, 2023
Accepted: November 13, 2023
Published: December 12, 2023

REFERENCES

1. Chiossone, L., Dumas, P.-Y., Vienne, M., and Vivier, E. (2018). Natural killer cells and other innate lymphoid cells in cancer. Nat. Rev. Immunol. *18*, 671–688.
2. Lanier, L.L. (2003). Natural killer cell receptor signaling. Curr. Opin. Immunol. *15*, 308–314.
3. Ruggeri, L., Capanni, M., Urbani, E., Perruccio, K., Shlomchik, W.D., Tosti, A., Posati, S., Rogaia, D., Frassoni, F., Aversa, F., et al. (2002). Effectiveness of donor natural killer cell alloreactivity in mismatched hematopoietic transplants. Science *295*, 2097–2100.
4. Liu, E., Marin, D., Banerjee, P., Macapinlac, H.A., Thompson, P., Basar, R., Nassif Kerbauy, L., Overman, B., Thall, P., Kaplan, M., et al. (2020). Use of CAR-transduced natural killer cells in CD19-positive lymphoid tumors. N. Engl. J. Med. *382*, 545–553.
5. Myers, J.A., and Miller, J.S. (2021). Exploring the NK cell platform for cancer immunotherapy. Nat. Rev. Clin. Oncol. *18*, 85–100.
6. Shimasaki, N., Jain, A., and Campana, D. (2020). NK cells for cancer immunotherapy. Nat. Rev. Drug Discov. *19*, 200–218.
7. Crinier, A., Milpied, P., Escalière, B., Piperoglou, C., Galluso, J., Balsamo, A., Spinelli, L., Cervera-Marzal, I., Ebbo, M., Girard-Madoux, M., et al. (2018). High-dimensional single-cell analysis identifies organ-specific signatures and conserved NK cell subsets in humans and mice. Immunity *49*, 971–986.e5.
8. Pfefferle, A., Netskar, H., Ask, E.H., Lorenz, S., Goodridge, J.P., Sohlberg, E., Clancy, T., and Malmberg, K.-J. (2019). A temporal transcriptional map of human natural killer cell differentiation. https://doi.org/10.1101/630657.
9. Smith, S.L., Kennedy, P.R., Stacey, K.B., Worboys, J.D., Yarwood, A., Seo, S., Solloa, E.H., Mistretta, B., Chatterjee, S.S., Gunaratne, P., et al. (2020). Diversity of peripheral blood human NK cells identified by single-cell RNA sequencing. Blood Adv. *4*, 1388–1406.
10. Yang, C., Siebert, J.R., Burns, R., Gerbec, Z.J., Bonacci, B., Rymaszewski, A., Rau, M., Riese, M.J., Rao, S., Carlson, K.-S., et al. (2019). Heterogeneity of human bone marrow and blood natural killer cells defined by single-cell transcriptome. Nat. Commun. *10*, 3931.
11. Cheng, S., Li, Z., Gao, R., Xing, B., Gao, Y., Yang, Y., Qin, S., Zhang, L., Ouyang, H., Du, P., et al. (2021). A pan-cancer single-cell transcriptional atlas of tumor infiltrating myeloid cells. Cell *184*, 792–809.e23.
12. Jerby-Arnon, L., Shah, P., Cuoco, M.S., Rodman, C., Su, M.-J., Melms, J.C., Leeson, R., Kanodia, A., Mei, S., Lin, J.-R., et al. (2018). A cancer cell program promotes T cell exclusion and resistance to checkpoint blockade. Cell *175*, 984–997.e24.
13. Zheng, L., Qin, S., Si, W., Wang, A., Xing, B., Gao, R., Ren, X., Wang, L., Wu, X., Zhang, J., et al. (2021). Pan-cancer single-cell landscape of tumor-infiltrating T cells. Science *374*, abe6474.
14. Kearney, C.J., Vervoort, S.J., Hogg, S.J., Ramsbottom, K.M., Freeman, A.J., Lalaoui, N., Pijpers, L., Michie, J., Brown, K.K., Knight, D.A., et al. (2018). Tumor immune evasion arises through loss of TNF sensitivity. Sci. Immunol. *3*, eaar3451.
15. Lawson, K.A., Sousa, C.M., Zhang, X., Kim, E., Akthar, R., Caumanns, J.J., Yao, Y., Mikolajewicz, N., Ross, C., Brown, K.R., et al. (2020). Functional genomic landscape of cancer-intrinsic evasion of killing by T cells. Nature *586*, 120–126.
16. Patel, S.J., Sanjana, N.E., Kishton, R.J., Eidizadeh, A., Vodnala, S.K., Cam, M., Gartner, J.J., Jia, L., Steinberg, S.M., Yamamoto, T.N., et al. (2017). Identification of essential genes for cancer immunotherapy. Nature *548*, 537–542.
17. Pan, D., Kobayashi, A., Jiang, P., Ferrari de Andrade, L.F., Tay, R.E., Luoma, A.M., Tsoucas, D., Qiu, X., Lim, K., Rao, P., et al. (2018). A major chromatin regulator determines resistance of tumor cells to T cell–mediated killing. Science *359*, 770–775.
18. Dufva, O., Koski, J., Maliniemi, P., Ianevski, A., Klievink, J., Leitner, J., Pölönen, P., Hohtari, H., Saeed, K., Hannunen, T., et al. (2020). Integrated drug profiling and CRISPR screening identify essential pathways for CAR T-cell cytotoxicity. Blood *135*, 597–609.
19. Singh, N., Lee, Y.G., Shestova, O., Ravikumar, P., Hayer, K.E., Hong, S.J., Lu, X.M., Pajarillo, R., Agarwal, S., Kuramitsu, S., et al. (2020). Impaired death receptor signaling in leukemia causes antigen-independent resistance by inducing CAR T-cell dysfunction. Cancer Discov. *10*, 552–567.
20. Yu, C., Mannan, A.M., Yvone, G.M., Ross, K.N., Zhang, Y.-L., Marton, M.A., Taylor, B.R., Crenshaw, A., Gould, J.Z., Tamayo, P., et al. (2016). High-throughput identification of genotype-specific cancer vulnerabilities in mixtures of barcoded tumor cell lines. Nat. Biotechnol. *34*, 419–423.

21. Sheffer, M., Lowry, E., Beelen, N., Borah, M., Amara, S.N.-A., Mader, C.C., Roth, J.A., Tsherniak, A., Freeman, S.S., Dashevsky, O., et al. (2021). Genome-scale screens identify factors regulating tumor cell responses to natural killer cells. Nat. Genet. *53*, 1196–1206.

22. Stoeckius, M., Zheng, S., Houck-Loomis, B., Hao, S., Yeung, B.Z., Mauck, W.M., Smibert, P., and Satija, R. (2018). Cell Hashing with barcoded antibodies enables multiplexing and doublet detection for single cell genomics. Genome Biol. *19*, 224.

23. Denman, C.J., Senyukov, V.V., Somanchi, S.S., Phatarpekar, P.V., Kopp, L.M., Johnson, J.L., Singh, H., Hurton, L., Maiti, S.N., Huls, M.H., et al. (2012). Membrane-bound IL-21 promotes sustained ex vivo proliferation of human natural killer cells. PLoS One *7*, e30264.

24. Lieberman, N.A.P., DeGolier, K., Haberthur, K., Chinn, H., Moyes, K.W., Bouchlaka, M.N., Walker, K.L., Capitini, C.M., and Crane, C.A. (2018). An uncoupling of canonical phenotypic markers and functional potency of ex vivo-expanded natural killer cells. Front. Immunol. *9*, 150.

25. Holmes, T.D., Pandey, R.V., Helm, E.Y., Schlums, H., Han, H., Campbell, T.M., Drashansky, T.T., Chiang, S., Wu, C.-Y., Tao, C., et al. (2021). The transcription factor Bcl11b promotes both canonical and adaptive NK cell differentiation. Sci. Immunol. *6*, eabc9801.

26. Merino, A., Zhang, B., Dougherty, P., Luo, X., Wang, J., Blazar, B.R., Miller, J.S., and Cichocki, F. (2019). Chronic stimulation drives human NK cell dysfunction and epigenetic reprograming. J. Clin. Invest. *129*, 3770–3785.

27. Gupta, P.K., Godec, J., Wolski, D., Adland, E., Yates, K., Pauken, K.E., Cosgrove, C., Ledderose, C., Junger, W.G., Robson, S.C., et al. (2015). CD39 expression identifies terminally exhausted CD8+ T cells. PLoS Pathog. *11*, e1005177.

28. Sade-Feldman, M., Yizhak, K., Bjorgaard, S.L., Ray, J.P., de Boer, C.G., Jenkins, R.W., Lieb, D.J., Chen, J.H., Frederick, D.T., Barzily-Rokni, M., et al. (2018). Defining T cell states associated with response to checkpoint immunotherapy in melanoma. Cell *175*, 998–1013.e20.

29. Simoni, Y., Becht, E., Fehlings, M., Loh, C.Y., Koo, S.-L., Teng, K.W.W., Yeong, J.P.S., Nahar, R., Zhang, T., Kared, H., et al. (2018). Bystander CD8+ T cells are abundant and phenotypically distinct in human tumour infiltrates. Nature *557*, 575–579.

30. Cuturi, M.C., Anegón, I., Sherman, F., Loudon, R., Clark, S.C., Perussia, B., and Trinchieri, G. (1989). Production of hematopoietic colony-stimulating factors by human natural killer cells. J. Exp. Med. *169*, 569–583.

31. Roda, J.M., Parihar, R., Magro, C., Nuovo, G.J., Tridandapani, S., and Carson, W.E., III (2006). Natural killer cells produce T cell–recruiting chemokines in response to antibody-coated tumor cells. Cancer Res. *66*, 517–526.

32. Fauriat, C., Long, E.O., Ljunggren, H.-G., and Bryceson, Y.T. (2010). Regulation of human NK-cell cytokine and chemokine production by target cell recognition. Blood *115*, 2167–2176.

33. La Manno, G., Soldatov, R., Zeisel, A., Braun, E., Hochgerner, H., Petukhov, V., Lidschreiber, K., Kastriti, M.E., Lönnerberg, P., Furlan, A., et al. (2018). RNA velocity of single cells. Nature *560*, 494–498.

34. Matsuo, Y., MacLeod, R.A., Uphoff, C.C., Drexler, H.G., Nishizaki, C., Katayama, Y., Kimura, G., Fujii, N., Omoto, E., Harada, M., et al. (1997). Two acute monocytic leukemia (AML-M5a) cell lines (MOLM-13 and MOLM-14) with interclonal phenotypic heterogeneity showing MLL-AF9 fusion resulting from an occult chromosome insertion, ins(11;9)(q23;p22p23). Leukemia *11*, 1469–1477.

35. Reddy, A., Zhang, J., Davis, N.S., Moffitt, A.B., Love, C.L., Waldrop, A., Leppa, S., Pasanen, A., Meriranta, L., Karjalainen-Lindsberg, M.-L., et al. (2017). Genetic and functional drivers of diffuse large B cell lymphoma. Cell *171*, 481–494.e15.

36. Cancer Genome Atlas Research Network, Ley, T.J., Miller, C., Ding, L., Raphael, B.J., Mungall, A.J., Robertson, A., Hoadley, K., Triche, T.J., Laird, P.W., et al. (2013). Genomic and epigenomic landscapes of adult de novo acute myeloid leukemia. N. Engl. J. Med. *368*, 2059–2074.

37. Efremova, M., Vento-Tormo, M., Teichmann, S.A., and Vento-Tormo, R. (2020). CellPhoneDB: inferring cell–cell communication from combined expression of multi-subunit ligand–receptor complexes. Nat. Protoc. *15*, 1484–1506.

38. Barretina, J., Caponigro, G., Stransky, N., Venkatesan, K., Margolin, A.A., Kim, S., Wilson, C.J., Lehár, J., Kryukov, G.V., Sonkin, D., et al. (2012). The Cancer Cell Line Encyclopedia enables predictive modelling of anticancer drug sensitivity. Nature *483*, 603–607.

39. Ghandi, M., Huang, F.W., Jané-Valbuena, J., Kryukov, G.V., Lo, C.C., McDonald, E.R., Barretina, J., Gelfand, E.T., Bielski, C.M., Li, H., et al. (2019). Next-generation characterization of the Cancer Cell Line Encyclopedia. Nature *569*, 503–508.

40. Meissner, T.B., Li, A., Biswas, A., Lee, K.-H., Liu, Y.-J., Bayir, E., Iliopoulos, D., van den Elsen, P.J., and Kobayashi, K.S. (2010). NLR family member NLRC5 is a transcriptional regulator of MHC class I genes. Proc. Natl. Acad. Sci. USA *107*, 13794–13799.

41. Kaer, L.V., Ashton-Rickardt, P.G., Ploegh, H.L., and Tonegawa, S. (1992). TAP1 mutant mice are deficient in antigen presentation, surface class I molecules, and CD4−8+ T cells. Cell *71*, 1205–1214.

42. Harjunpää, H., Llort Asens, M., Guenther, C., and Fagerholm, S.C. (2019). Cell adhesion molecules and their roles and regulation in the immune and tumor microenvironment. Front. Immunol. *10*, 1078.

43. Schneider, M., Al-Shareffi, E., and Haltiwanger, R.S. (2017). Biological functions of fucose in mammals. Glycobiology *27*, 601–618.

44. Voss, M., Künzel, U., Higel, F., Kuhn, P.-H., Colombo, A., Fukumori, A., Haug-Kröper, M., Klier, B., Grammer, G., Seidl, A., et al. (2014). Shedding of glycan-modifying enzymes by signal peptide peptidase-like 3 (SPPL3) regulates cellular N-glycosylation. EMBO J. *33*, 2890–2905.

45. Jongsma, M.L.M., de Waard, A.A., Raaben, M., Zhang, T., Cabukusta, B., Platzer, R., Blomen, V.A., Xagara, A., Verkerk, T., Bliss, S., et al. (2021). The SPPL3-defined glycosphingolipid repertoire orchestrates HLA class I-mediated immune responses. Immunity *54*, 132–150.e9.

46. Rillahan, C.D., Antonopoulos, A., Lefort, C.T., Sonon, R., Azadi, P., Ley, K., Dell, A., Haslam, S.M., and Paulson, J.C. (2012). Global metabolic inhibitors of sialyl- and fucosyltransferases remodel the glycome. Nat. Chem. Biol. *8*, 661–668.

47. Burkart, M.D., Vincent, S.P., Düffels, A., Murray, B.W., Ley, S.V., and Wong, C.H. (2000). Chemo-enzymatic synthesis of fluorinated sugar nucleotide: useful mechanistic Probes for glycosyltransferases. Bioorg. Med. Chem. *8*, 1937–1946.

48. Keats, J.J., Fonseca, R., Chesi, M., Schop, R., Baker, A., Chng, W.-J., Van Wier, S.V., Tiedemann, R., Shi, C.-X., Sebag, M., et al. (2007). Promiscuous mutations activate the noncanonical NF-κB pathway in multiple myeloma. Cancer Cell *12*, 131–144.

49. Liao, G., Zhang, M., Harhaj, E.W., and Sun, S.C. (2004). Regulation of the NF-κB-inducing kinase by tumor necrosis factor Receptor-associated Factor 3-induced Degradation*. J. Biol. Chem. *279*, 26243–26250.

50. Micheau, O., Lens, S., Gaide, O., Alevizopoulos, K., and Tschopp, J. (2001). NF-κB signals induce the expression of c-FLIP. Mol. Cell. Biol. *21*, 5299–5305.

51. Ferrando, A.A., Neuberg, D.S., Staunton, J., Loh, M.L., Huard, C., Raimondi, S.C., Behm, F.G., Pui, C.-H., Downing, J.R., Gilliland, D.G., et al. (2002). Gene expression signatures define novel oncogenic pathways in T cell acute lymphoblastic leukemia. Cancer Cell *1*, 75–87.

52. Liu, Y., Easton, J., Shao, Y., Maciaszek, J., Wang, Z., Wilkinson, M.R., McCastlain, K., Edmonson, M., Pounds, S.B., Shi, L., et al. (2017). The genomic landscape of pediatric and young adult T-lineage acute lymphoblastic leukemia. Nat. Genet. *49*, 1211–1218.

53. Roels, J., Thénoz, M., Szarzyńska, B., Landfors, M., De Coninck, S.D., Demoen, L., Provez, L., Kuchmiy, A., Strubbe, S., Reunes, L., et al. (2020). Aging of preleukemic thymocytes drives CpG island hypermethylation in T-cell acute lymphoblastic leukemia. Blood Cancer Discov. *1*, 274–289.

54. Datlinger, P., Rendeiro, A.F., Schmidl, C., Krausgruber, T., Traxler, P., Klughammer, J., Schuster, L.C., Kuchler, A., Alpar, D., and Bock, C.

(2017). Pooled CRISPR screening with single-cell transcriptome readout. Nat. Methods *14*, 297–301.

55. Papalexi, E., Mimitou, E.P., Butler, A.W., Foster, S., Bracken, B., Mauck, W.M., Wessels, H.-H., Hao, Y., Yeung, B.Z., Smibert, P., et al. (2021). Characterizing the molecular regulation of inhibitory immune checkpoints with multimodal single-cell screens. Nat. Genet. *53*, 322–331.
56. Dersh, D., Phelan, J.D., Gumina, M.E., Wang, B., Arbuckle, J.H., Holly, J., Kishton, R.J., Markowitz, T.E., Seedhom, M.O., Fridlyand, N., et al. (2021). Genome-wide screens identify lineage- and tumor-specific genes modulating MHC-I- and MHC-II-restricted immunosurveillance of human lymphomas. Immunity *54*, 116–131.e10.
57. Henry, C.M., and Martin, S.J. (2017). Caspase-8 acts in a non-enzymatic role as a scaffold for assembly of a pro-inflammatory "FADDosome" complex upon TRAIL stimulation. Mol. Cell *65*, 715–729.e5.
58. Kreuz, S., Siegmund, D., Rumpf, J.-J., Samel, D., Leverkus, M., Janssen, O., Häcker, G., Dittrich-Breiholz, O., Kracht, M., Scheurich, P., et al. (2004). NFκB activation by Fas is mediated through FADD, caspase-8, and RIP and is inhibited by FLIP. J. Cell Biol. *166*, 369–380.
59. Annunziata, C.M., Davis, R.E., Demchenko, Y., Bellamy, W., Gabrea, A., Zhan, F., Lenz, G., Hanamura, I., Wright, G., Xiao, W., et al. (2007). Frequent engagement of the classical and alternative NF-κB pathways by diverse genetic abnormalities in multiple myeloma. Cancer Cell *12*, 115–130.
60. Herishanu, Y., Pérez-Galán, P., Liu, D., Biancotto, A., Pittaluga, S., Vire, B., Gibellini, F., Njuguna, N., Lee, E., Stennett, L., et al. (2011). The lymph node microenvironment promotes B-cell receptor signaling, NF-κB activation, and tumor proliferation in chronic lymphocytic leukemia. Blood *117*, 563–574.
61. Loetscher, M., Gerber, B., Loetscher, P., Jones, S.A., Piali, L., Clark-Lewis, I., Baggiolini, M., and Moser, B. (1996). Chemokine receptor specific for IP10 and mig: structure, function, and expression in activated T-lymphocytes. J. Exp. Med. *184*, 963–969.
62. Loetscher, P., Seitz, M., Clark-Lewis, I., Baggiolini, M., and Moser, B. (1996). Activation of NK cells by CC chemokines. Chemotaxis, Ca2+ mobilization, and enzyme release. J. Immunol. *156*, 322–327.
63. Schall, T.J., Bacon, K., Toy, K.J., and Goeddel, D.V. (1990). Selective attraction of monocytes and T lymphocytes of the memory phenotype by cytokine RANTES. Nature *347*, 669–671.
64. Taub, D.D., Lloyd, A.R., Conlon, K., Wang, J.M., Ortaldo, J.R., Harada, A., Matsushima, K., Kelvin, D.J., and Oppenheim, J.J. (1993). Recombinant human interferon-inducible protein 10 is a chemoattractant for human monocytes and T lymphocytes and promotes T cell adhesion to endothelial cells. J. Exp. Med. *177*, 1809–1814.
65. Baessler, T., Charton, J.E., Schmiedel, B.J., Grünebach, F., Krusch, M., Wacker, A., Rammensee, H.G., and Salih, H.R. (2010). CD137 ligand mediates opposite effects in human and mouse NK cells and impairs NK-cell reactivity against human acute myeloid leukemia cells. Blood *115*, 3058–3069.
66. Costanzo, M.C., Kim, D., Creegan, M., Lal, K.G., Ake, J.A., Currier, J.R., Streeck, H., Robb, M.L., Michael, N.L., Bolton, D.L., et al. (2018). Transcriptomic signatures of NK cells suggest impaired responsiveness in HIV-1 infection and increased activity post-vaccination. Nat. Commun. *9*, 1212.
67. Turaj, A.H., Cox, K.L., Penfold, C.A., French, R.R., Mockridge, C.I., Willoughby, J.E., Tutt, A.L., Griffiths, J., Johnson, P.W.M., Glennie, M.J., et al. (2018). Augmentation of CD134 (OX40)-dependent NK antitumour activity is dependent on antibody cross-linking. Sci. Rep. *8*, 2278.
68. Notarbartolo, S., Ranzani, V., Bandera, A., Gruarin, P., Bevilacqua, V., Putignano, A.R., Gobbini, A., Galeota, E., Manara, C., Bombaci, M., et al. (2021). Integrated longitudinal immunophenotypic, transcriptional, and repertoire analyses delineate immune responses in patients with COVID-19. Sci. Immunol. *6*, eabg5021.
69. Krämer, B., Knoll, R., Bonaguro, L., ToVinh, M., Raabe, J., Astaburuaga-García, R., Schulte-Schrepping, J., Kaiser, K.M., Rieke, G.J., Bischoff, J., et al. (2021). Early IFN-α signatures and persistent dysfunction are distinguishing features of NK cells in severe COVID-19. Immunity *54*, 2650–2669.e14.
70. Baltz, K.M., Krusch, M., Bringmann, A., Brossart, P., Mayer, F., Kloss, M., Baessler, T., Kumbier, I., Peterfi, A., Kupka, S., et al. (2007). Cancer immunoediting by GITR (glucocorticoid-induced TNF-related protein) ligand in humans: NK cell/tumor cell interactions. FASEB J. *21*, 2442–2454.
71. Piontek, G.E., Taniguchi, K., Ljunggren, H.G., Grönberg, A., Kiessling, R., Klein, G., and Kärre, K. (1985). YAC-1 MHC class I variants reveal an association between decreased NK sensitivity and increased H-2 expression after interferon treatment or in vivo passage. J. Immunol. *135*, 4281–4288.
72. Trinchieri, G., and Santoli, D. (1978). Anti-viral activity induced by culturing lymphocytes with tumor-derived or virus-transformed cells. Enhancement of human natural killer cell activity by interferon and antagonistic inhibition of susceptibility of target cells to lysis. J. Exp. Med. *147*, 1314–1333.
73. Maki, G., Klingemann, H.-G., Martinson, J.A., and Tam, Y.K. (2001). Factors regulating the cytotoxic activity of the human natural killer cell line, NK-92. J. Hematother. Stem Cell Res. *10*, 369–383.
74. Pech, M.F., Fong, L.E., Villalta, J.E., Chan, L.J., Kharbanda, S., O'Brien, J.J., McAllister, F.E., Firestone, A.J., Jan, C.H., and Settleman, J. (2019). Systematic identification of cancer cell vulnerabilities to natural killer cell-mediated immune surveillance. eLife *8*, e47362.
75. Benci, J.L., Johnson, L.R., Choa, R., Xu, Y., Qiu, J., Zhou, Z., Xu, B., Ye, D., Nathanson, K.L., June, C.H., et al. (2019). Opposing functions of interferon coordinate adaptive and innate immune responses to cancer immune checkpoint blockade. Cell *178*, 933–948.e14.
76. Weichselbaum, R.R., Ishwaran, H., Yoon, T., Nuyten, D.S.A., Baker, S.W., Khodarev, N., Su, A.W., Shaikh, A.Y., Roach, P., Kreike, B., et al. (2008). An interferon-related gene signature for DNA damage resistance is a predictive marker for chemotherapy and radiation for breast cancer. Proc. Natl. Acad. Sci. USA *105*, 18490–18495.
77. Zaretsky, J.M., Garcia-Diaz, A., Shin, D.S., Escuin-Ordinas, H., Hugo, W., Hu-Lieskovan, S., Torrejon, D.Y., Abril-Rodriguez, G., Sandoval, S., Barthly, L., et al. (2016). Mutations associated with acquired resistance to PD-1 blockade in melanoma. N. Engl. J. Med. *375*, 819–829.
78. Freeman, A.J., Vervoort, S.J., Ramsbottom, K.M., Kelly, M.J., Michie, J., Pijpers, L., Johnstone, R.W., Kearney, C.J., and Oliaro, J. (2019). Natural killer cells suppress T cell-associated tumor immune evasion. Cell Rep. *28*, 2784–2794.e5.
79. Pende, D., Spaggiari, G.M., Marcenaro, S., Martini, S., Rivera, P., Capobianco, A., Falco, M., Lanino, E., Pierri, I., Zambello, R., et al. (2005). Analysis of the receptor-ligand interactions in the natural killer–mediated lysis of freshly isolated myeloid or lymphoblastic leukemias: evidence for the involvement of the poliovirus receptor (CD155) and Nectin-2 (CD112). Blood *105*, 2066–2073.
80. Nowbakht, P., Ionescu, M.C., Rohner, A., Kalberer, C.P., Rossy, E., Mori, L., Cosman, D., De Libero, G., and Wodnar-Filipowicz, A. (2005). Ligands for natural killer cell–activating receptors are expressed upon the maturation of normal myelomonocytic cells but at low levels in acute myeloid leukemias. Blood *105*, 3615–3622.
81. Paczulla, A.M., Rothfelder, K., Raffel, S., Konantz, M., Steinbacher, J., Wang, H., Tandler, C., Mbarga, M., Schaefer, T., Falcone, M., et al. (2019). Absence of NKG2D ligands defines leukaemia stem cells and mediates their immune evasion. Nature *572*, 254–259.
82. Vredevoogd, D.W., Kuilman, T., Ligtenberg, M.A., Boshuizen, J., Stecker, K.E., de Bruijn, B., Krijgsman, O., Huang, X., Kenski, J.C.N., Lacroix, R., et al. (2019). Augmenting immunotherapy impact by lowering tumor TNF cytotoxicity threshold. Cell *178*, 585–599.e15.
83. Morimoto, Y., Yamashita, N., Daimon, T., Hirose, H., Yamano, S., Haratake, N., Ishikawa, S., Bhattacharya, A., Fushimi, A., Ahmad, R., et al. (2023). MUC1-C is a master regulator of MICA/B NKG2D ligand and exosome secretion in human cancer cells. J. Immunother. Cancer *11*, e006238.
84. Shinkawa, T., Nakamura, K., Yamane, N., Shoji-Hosaka, E., Kanda, Y., Sakurada, M., Uchida, K., Anazawa, H., Satoh, M., Yamasaki, M., et al. (2003). The absence of fucose but not the presence of galactose or

bisecting N-acetylglucosamine of human IgG1 complex-type oligosaccharides shows the critical role of enhancing antibody-dependent cellular cytotoxicity. J. Biol. Chem. *278*, 3466–3473.

85. Shields, R.L., Lai, J., Keck, R., O'Connell, L.Y., Hong, K., Meng, Y.G., Weikert, S.H.A., and Presta, L.G. (2002). Lack of fucose on human IgG1 N-linked oligosaccharide improves binding to human Fcgamma RIII and antibody-dependent cellular toxicity. J. Biol. Chem. *277*, 26733–26740.
86. Wisnovsky, S., Möckl, L., Malaker, S.A., Pedram, K., Hess, G.T., Riley, N.M., Gray, M.A., Smith, B.A.H., Bassik, M.C., Moerner, W.E., et al. (2021). Genome-wide CRISPR screens reveal a specific ligand for the glycan-binding immune checkpoint receptor Siglec-7. Proc. Natl. Acad. Sci. USA *118*, e2015024118.
87. Daly, J., Sarkar, S., Natoni, A., Stark, J.C., Riley, N.M., Bertozzi, C.R., Carlsten, M., and O'Dwyer, M.E. (2022). Targeting hypersialylation in multiple myeloma represents a novel approach to enhance NK cell–mediated tumor responses. Blood Adv. *6*, 3352–3366.
88. Pan, R., Ryan, J., Pan, D., Wucherpfennig, K.W., and Letai, A. (2022). Augmenting NK cell-based immunotherapy by targeting mitochondrial apoptosis. Cell *185*, 1521–1538.e18.
89. Upadhyay, R., Boiarsky, J.A., Pantsulaia, G., Svensson-Arvelund, J., Lin, M.J., Wroblewska, A., Bhalla, S., Scholler, N., Bot, A., Rossi, J.M., et al. (2021). A critical role for fas-mediated off-target tumor killing in T cell immunotherapy. Cancer Discov. *11*, 599–613.
90. Li, W., Xu, H., Xiao, T., Cong, L., Love, M.I., Zhang, F., Irizarry, R.A., Liu, J.S., Brown, M., and Liu, X.S. (2014). MAGeCK enables robust identification of essential genes from genome-scale CRISPR/Cas9 knockout screens. Genome Biol. *15*, 554.
91. Gu, Z., Eils, R., and Schlesner, M. (2016). Complex heatmaps reveal patterns and correlations in multidimensional genomic data. Bioinformatics *32*, 2847–2849.
92. Subramanian, A., Tamayo, P., Mootha, V.K., Mukherjee, S., Ebert, B.L., Gillette, M.A., Paulovich, A., Pomeroy, S.L., Golub, T.R., Lander, E.S., et al. (2005). Gene set enrichment analysis: a knowledge-based approach for interpreting genome-wide expression profiles. Proc. Natl. Acad. Sci. USA *102*, 15545–15550.
93. Korotkevich, G., Sukhov, V., and Sergushichev, A. (2019). Fast gene set enrichment analysis. https://doi.org/10.1101/060012.
94. Stuart, T., Butler, A., Hoffman, P., Hafemeister, C., Papalexi, E., Mauck, W.M., Hao, Y., Stoeckius, M., Smibert, P., and Satija, R. (2019). Comprehensive integration of single-cell data. Cell *177*, 1888–1902.e21.
95. McInnes, L., Healy, J., and Melville, J. (2020). UMAP: uniform manifold approximation and projection for dimension reduction. https://doi.org/10.48550/arXiv.1802.03426.
96. Aran, D., Looney, A.P., Liu, L., Wu, E., Fong, V., Hsu, A., Chak, S., Naikawadi, R.P., Wolters, P.J., Abate, A.R., et al. (2019). Reference-based analysis of lung single-cell sequencing reveals a transitional profibrotic macrophage. Nat. Immunol. *20*, 163–172.
97. Bergen, V., Lange, M., Peidli, S., Wolf, F.A., and Theis, F.J. (2020). Generalizing RNA velocity to transient cell states through dynamical modeling. Nat. Biotechnol. *38*, 1408–1414.
98. Hänzelmann, S., Castelo, R., and Guinney, J. (2013). GSVA: gene set variation analysis for microarray and RNA-Seq data. BMC Bioinformatics *14*, 7.
99. Chapuy, B., Stewart, C., Dunford, A.J., Kim, J., Kamburov, A., Redd, R.A., Lawrence, M.S., Roemer, M.G.M., Li, A.J., Ziepert, M., et al. (2018). Molecular subtypes of diffuse large B cell lymphoma are associated with distinct pathogenic mechanisms and outcomes. Nat. Med. *24*, 679–690.
100. Manojlovic, Z., Christofferson, A., Liang, W.S., Aldrich, J., Washington, M., Wong, S., Rohrer, D., Jewell, S., Kittles, R.A., Derome, M., et al. (2017). Comprehensive molecular profiling of 718 Multiple myelomas reveals significant differences in mutation frequencies between African and European descent cases. PLOS Genet. *13*, e1007087.
101. Stunnenberg, H.G.; International Human Epigenome Consortium, and Hirst, M. (2016). The international human epigenome consortium: A blueprint for scientific collaboration and discovery. Cell *167*, 1145–1149.
102. Dunham, I., Kundaje, A., Aldred, S.F., Collins, P.J., Davis, C.A., Doyle, F., Epstein, C.B., Frietze, S., Harrow, J., and Kaul, R. (2012). An integrated encyclopedia of DNA elements in the human genome. Nature *489*, 57–74.
103. Pölönen, P., Mehtonen, J., Lin, J., Liuksiala, T., Häyrynen, S., Teppo, S., Mäkinen, A., Kumar, A., Malani, D., Pohjolainen, V., et al. (2019). Hemap: an interactive online resource for characterizing molecular phenotypes across hematologic malignancies. Cancer Res. *79*, 2466–2479.
104. Dufva, O., Pölönen, P., Brück, O., Keränen, M.A.I., Klievink, J., Mehtonen, J., Huuhtanen, J., Kumar, A., Malani, D., Siitonen, S., et al. (2020). Immunogenomic landscape of hematological malignancies. Cancer Cell *38*, 380–399.e13.
105. Sanjana, N.E., Shalem, O., and Zhang, F. (2014). Improved vectors and genome-wide libraries for CRISPR screening. Nat. Methods *11*, 783–784.
106. Doench, J.G., Fusi, N., Sullender, M., Hegde, M., Vaimberg, E.W., Donovan, K.F., Smith, I., Tothova, Z., Wilen, C., Orchard, R., et al. (2016). Optimized sgRNA design to maximize activity and minimize off-target effects of CRISPR-Cas9. Nat. Biotechnol. *34*, 184–191.
107. Sanson, K.R., Hanna, R.E., Hegde, M., Donovan, K.F., Strand, C., Sullender, M.E., Vaimberg, E.W., Goodale, A., Root, D.E., Piccioni, F., et al. (2018). Optimized libraries for CRISPR-Cas9 genetic screens with multiple modalities. Nat. Commun. *9*, 5416.
108. Shalem, O., Sanjana, N.E., Hartenian, E., Shi, X., Scott, D.A., Mikkelson, T.S., Heckl, D., Ebert, B.L., Root, D.E., Doench, J.G., et al. (2014). Genome-scale CRISPR-Cas9 knockout screening in human cells. Science *343*, 84–87.
109. Dashevsky, O., De Matos Simoes, R., Shirasaki, R., Sheffer, M., Dhimolea, E., Gandolfi, S., Tang, H., Downey-Kopyscinski, S.L., Bariteau, M., Sorrell, J., et al. (2020). Use of olfactory receptor genes as controls for genome-scale CRISPR functional genomic studies to define treatment resistance mechanisms. Blood *136*, 36–49.
110. de Matos Simoes, R., Shirasaki, R., Downey-Kopyscinski, S.L., Matthews, G.M., Barwick, B.G., Gupta, V.A., Dupéré-Richer, D., Yamano, S., Hu, Y., Sheffer, M., et al. (2023). Genome-scale functional genomics identify genes preferentially essential for multiple myeloma cells compared to other neoplasias. Nat. Cancer *4*, 754–773.
111. Okada, M., Chikuma, S., Kondo, T., Hibino, S., Machiyama, H., Yokosuka, T., Nakano, M., and Yoshimura, A. (2017). Blockage of core fucosylation reduces cell-surface expression of PD-1 and promotes anti-tumor immune responses of T cells. Cell Rep. *20*, 1017–1028.
112. Alda-Catalinas, C., Bredikhin, D., Hernando-Herraez, I., Santos, F., Kubinyecz, O., Eckersley-Maslin, M.A., Stegle, O., and Reik, W. (2020). A single-cell transcriptomics CRISPR-activation screen identifies epigenetic regulators of the zygotic genome activation program. Cell Syst. *11*, 25–41.e9.
113. Hill, A.J., McFaline-Figueroa, J.L., Starita, L.M., Gasperini, M.J., Matreyek, K.A., Packer, J., Jackson, D., Shendure, J., and Trapnell, C. (2018). On the design of CRISPR-based single-cell molecular screens. Nat. Methods *15*, 271–274.
114. Ritchie, M.E., Phipson, B., Wu, D., Hu, Y., Law, C.W., Shi, W., and Smyth, G.K. (2015). limma powers differential expression analyses for RNA-sequencing and microarray studies. Nucleic Acids Res. *43*, e47.

STAR★METHODS

KEY RESOURCES TABLE

REAGENT or RESOURCE	SOURCE	IDENTIFIER
Antibodies		
NKp46 APC monoclonal antibody	BD Biosciences	Cat# BDB558051 RRID: AB_398653
CD314 (NKG2D) APC monoclonal antibody	Miltenyi Biotec	Cat# 130-117-830 RRID: AB_2733372
CD3 FITC monoclonal antibody	Miltenyi Biotec	Cat# 130-098-162 RRID:AB_2726231
CD56 PE-Cy7	BD Biosciences	Cat# BDB335809 RRID:AB_399984
NKp30 A488 monoclonal antibody (Clone 210845)	Thermo Fisher	Cat# FAB1849G RRID:AB_10889633
CD43 PE (clone 1G10)	BD Biosciences	Cat# 560199 RRID:AB_1645655
Anti-CD43 antibody (clone MEM-59)	Abcam	Cat# ab9088 RRID:AB_446600
Mouse IgG1 isotype control (clone 15-6E10A7)	Abcam	Cat# ab170190 RRID:AB_2736870
Purified NA/LE mouse anti-human MUC1 blocking antibody (clone VU4H5)	Cell Signaling	Cat# 4538 RRID: AB_2148549
Purified NA/LE IgG1κ isotype control (clone G3A1)	Cell Signaling	Cat# 5415S RRID:AB_10829607
Purified NA/LE anti-CD162 blocking antibody (clone KPL-1 RUO)	BD Pharmingen	Cat# 556052 RRID:AB_396323
Purified NA/LE mouse IgG1κ isotype control	BD Pharmingen	Cat# 554721 RRID:AB_395530
TotalSeq™-A antibodies	BioLegend See Table S1B for HTO sequences	Cat# 394601-29 RRID:AB_2750015 to AB_2750028
Bacterial and virus strains		
ElectroMAX Stbl4 Competent Cells	Invitrogen	Cat# 11635018
Endura ElectroCompetent Cells	Lucigen	Cat# 60242-1
Biological samples		
Human PBMCs	Finnish Red Cross Blood Service	N/A
Human PBMCs	Specimen Bank Brigham and Women's Hospital	N/A
Chemicals, peptides, and recombinant proteins		
Cell Culture Phosphate Buffered Saline (PBS)	Corning	Cat# 21040CV
Fetal Bovine Serum Tetracycline Negative (FBS)	Gemini Bio-Products,	Cat# 100-800
Bovine Serum Albumin	New England Biolabs	Cat# B9000S
RPMI 1640	Gibco	Cat# 11875119
RPMI 1640 Medium, no phenol red	Gibco	Cat# 11835030
GMP SCGM	Cellgenix Usa	Cat# 20802-0500
GlutaMAX, 200 mM	Gibco	Cat# 35050061
Human recombinant IL-2	R&D Systems	Cat# 202-IL-050
RBC Lysis Buffer for Human Red Blood Cells	VWR	Cat# IBB-197
Trypsin-EDTA (0.05%), phenol red	Gibco	Cat# 25300120
Opti-MEM I Reduced Serum Medium	Gibco	Cat# 31985070
Hepes	Gibco	Cat# 15630080
Lipofectamine 2000	Thermo Fisher Scientific	Cat# 11668030
Polybrene	Sigma Aldrich	Cat# TR-1003-G
Puromycin Dihydrochloride	Thermo Fisher Scientific	Cat# BP2956100
Blasticidin	Gibco	Cat# R21001
Ampicillin	Sigma Aldrich	Cat# A5354
Penicillin-Streptomycin Solution	Corning	Cat# 30001CI

(*Continued on next page*)

Continued

REAGENT or RESOURCE	SOURCE	IDENTIFIER
2F-Peracetyl-Fucose	Sigma Aldrich	Cat# 344827
Lens Culinaris Agglutinin (LCA) fluorescein	Vector	Cat#FL-1041-5
Calcein AM	Invitrogen	Cat# C1430
Calcein AM DW buffer	R&D systems	Cat# 4892-010-02
NP40 cell lysis buffer	Invitrogen	Cat# FNN0021
QIAGEN Proteinase K	Qiagen	Cat# 19133
TWEEN-20	Sigma Aldrich	Cat# P9416
Human TruStain FcX™	BioLegend	Cat# 422302
Cell Staining Buffer	BioLegend	Cat# 420201
Critical commercial assays		
Blood & Cell Culture DNA Midi Kit	Qiagen	Cat# 13343
Blood & Cell Culture DNA Maxi Kit	Qiagen	Cat# 13362
QIAquick Gel Extraction Kit	Qiagen	Cat# 28706
QIamp DNA Mini Kit	Qiagen	Cat# 51304
MycoAlert KIT	Lonza	Cat# LT07-710
CellTiterGlo	Promega	Cat# G7572
One-Glo™ Luciferase Assay System	Promega	Cat# E6120
Phusion High-Fidelity PCR Master Mix with HF Buffer	New England Biolabs	Cat# M0531L
NK Cell Isolation Kit, human	Miltenyi Biotec	Cat# 130-092-657
RosetteSep Human CD3 Depletion Cocktail	StemCell Technologies	Cat# 15661
Bio-Plex Pro Human Cytokine 27-plex Assay	BioRad	Cat# M500KCAF0Y
Chromium Next GEM Single Cell 3' Kit v3.0 and v3.1	10x Genomics	PN-1000268
Chromium Next GEM Chip G Single Cell Kit	10x Genomics	PN-1000127
Dual Index Kit TT Set A	10x Genomics	PN-1000215
Experimental models: Cell lines		
Lenti-X™ 293T Cell Line	Takara Bio	Cat# 632180
KHYG1	DSMZ	Cat# ACC 725 RRID:CVCL_2976
MM1.S-Cas9	B. Ebert's lab	N/A
KMS11-Cas9	Broad Institute, MIT	N/A
LP-1-Cas9	Broad Institute, MIT	N/A
LP-1-dCas9/VP64	Broad Institute, MIT	N/A
KMS11-dCas9/VP64	Broad Institute, MIT	N/A
K562-Cas9	This study	N/A
MOLM14-Cas9	This study	N/A
SUDHL4-Cas9	This study	N/A
NALM6-Cas9	Dufva et al.[18]	N/A
K562-luc	This study	N/A
SUDHL4-luc	Dufva et al.[18]	N/A
NALM6-luc	Dufva et al.[18]	N/A
K562-mbIL21-41BBL	Kiadis, a Sanofi Company	Cat# CSTX-002
PRISM cell line panel	Broad Institute, MIT	see Table S3
Cell line panel used in co-culture scRNA-seq	N/A	see Table S1
Oligonucleotides		
Genome-scale CRISPR screen primers	See Table S4 tab Primers	N/A
Focused library CRISPR LOF sgRNAs	See Table S4 tab P	N/A
Single gene validation CRISPR LOF sgRNAs	See Table S4 tab Q	N/A

(*Continued on next page*)

Continued

REAGENT or RESOURCE	SOURCE	IDENTIFIER
CROP-seq sgRNAs	See Table S6	N/A
Recombinant DNA		
lentiCas9-Blast	Addgene	Cat# 52962 RRID:Addgene_52962
lentiGuide-Puro	Addgene	Cat# 52963 RRID:Addgene_52963
psPAX2	Addgene	Cat#12260 RRID:Addgene_12260
pMD2.G	Addgene	Cat# 12259 RRID:Addgene_12259
pCMV-VSV-G	Addgene	Cat#8454 RRID:Addgene_8454
Lenti dCAS9-VP64_Blast	Addgene	Cat# 61425 RRID:Addgene_61425
Brunello human library	Addgene	Cat# 73178 RRID:Addgene_73178
Human CRISPR Activation Pooled sgRNA Library (Calabrese library)	Addgene	Cat# 92377; 92378
GeCKO v2 human library	Addgene	Cat# 1000000049
pLenti PGK V5-LUC Neo (w623-2)	Addgene	Cat# 21471 RRID:Addgene_21471
CROPseq-Guide-Puro	Addgene	Cat# 86708 RRID:Addgene_86708
CROP-sgRNA-MS2	Addgene	Cat# 153457 RRID:Addgene_153457
lentiCRISPRv2	Addgene	Cat# 52961 RRID:Addgene_52961
Software and algorithms		
cutadapt (v.1.9.1)	https://github.com/marcelm/cutadapt/; bowtie2 Lagmead et al.	https://sourceforge.net/projects/bowtie-bio/
PRISM 8	GraphPad	https://www.graphpad.com
FlowJo (v9.7.6)	Tree Star	https://www.flowjo.com/
MAGeCK (v0.5.2 and v0.5.7)	Li et al.[90]	https://sourceforge.net/projects/mageck/
RStudio	Integrated Development for R. RStudio, PBC, Boston, MA	http://www.rstudio.com/
Cell Ranger (v3.1 and v6.0.2)	10x Genomics	N/A
bcl2fastq (v2.2.0)	Illumina	N/A
CITE-seq-Count	Stoeckius et al.[22]	https://hoohm.github.io/CITE-seq-Count/
Bioconductor (v3.13)	N/A	http://www. bioconductor.org/
ggplot2	N/A	https://ggplot2. tidyverse.org
ComplexHeatmap	Gu et al.[91]	https://bioconductor.org/packages/release/bioc/html/ComplexHeatmap.html
MSigDB	Subramanian et al.[92]	https://www.gsea-msigdb.org/gsea/msigdb
fgsea	Korotkevich et al.[93]	https://bioconductor.org/packages/release/bioc/html/fgsea.html
R	R Core Team	https://www.r-project.orgs
Seurat (v4.0.4)	Stuart et al.[94]	https://cran.r-project. org/web/packages/Seurat/index.html
umap	McInnes et al.[95]	https://github.com/lmcinnes/umap
SingleR (v1.6.1)	Aran et al.[96]	https://github.com/dviraran/SingleR
CellPhoneDB	Efremova et al.[37]	https://github.com/ Teichlab/cellphonedb
velocyto (v0.17.17)	La Manno et al.[33]	https://velocyto.org/
scVelo (v0.2.5)	Bergen et al.[97]	https://scvelo.readthedocs.io/en/stable/
GSVA (v1.24.0)	Hänzelmann et al.[98]	https://bioconductor.org/packages/release/bioc/html/GSVA.html
DescTools (v0.99.43)	N/A	https://cran.r-project.org/web/packages/DescTools/index.html

(*Continued on next page*)

Continued

REAGENT or RESOURCE	SOURCE	IDENTIFIER
survival (v3.5-5)	N/A	https://cran.r-project.org/web/packages/survival/index.html
OrderedList (v1.64.0)	N/A	https://www.bioconductor.org/packages/release/bioc/html/OrderedList.html
Deposited Data		
Raw sequencing data from co-culture scRNA-seq and CROP-seq experiments	This study	EGA: EGAS00001007272
Processed data from co-culture scRNA-seq and CROP-seq experiments	This study	ArrayExpress: E-MTAB-13204
Genome-wide CRISPR screen data	This study	Synapse https://doi.org/10.7303/syn52600685
CCLE multi-omic data	Barretina et al.[38]; Ghandi et al.[39]	https://depmap.org/portal/download/all/
DLBCL gene expression, genetic alteration, and clinical data	Reddy et al.[35]	EGA: EGAS00001002606
DLBCL gene expression, genetic alteration, and clinical data	Chapuy et al.[99]	GEO: GSE98588
TCGA AML and DLBCL	TCGA Research Network	dbGaP: phs000178.v8.p7
CoMMpass MM gene expression, genetic alteration, and clinical data	Manojlovic et al.[100]	https://research.themmrf.org/rp/download
T-ALL gene expression, genetic alteration, and clinical data	Liu et al.[52]	dbGaP: phs000218.v26.p8
T-ALL methylation data	Roels et al.[53]	GEO: GSE155333
CRISPR screening data of MHC-I regulators	Dersh et al.[56]	N/A
Normal cell type gene expression data from Blueprint and ENCODE	Stunnenberg et al.[101]; Dunham et al.[102]	https://github.com/dviraran/SingleR/blob/master/data/blueprint_encode.rda
Patient survival data from Hemap dataset	Pölönen et al.[103]; Dufva, Pölönen et al.[104]	Synapse https://doi.org/10.7303/syn21991014;http://hemap.uta.fi

RESOURCE AVAILABILITY

Lead contact

Further information and requests for resources and reagents should be directed to and will be fulfilled by the lead contact, Satu Mustjoki (satu.mustjoki@helsinki.fi) and the co-corresponding author Constantine Mitsiades (constantine_mitsiades@dfci.harvard.edu).

Materials availability

Materials are available upon request from the lead contact. This study did not generate new unique reagents.

Data and code availability

The results of the study can be interactively explored at: https://immunogenomics.shinyapps.io/nkheme/. Raw scRNA-seq data generated in this study are available at EGA: EGAS00001007272) Processed scRNA-seq data are available at ArrayExpress: E-MTAB-13204. Genome-scale CRISPR screen data (sgRNA count matrices) are available at Synapse: syn52600685 (https://doi.org/10.7303/syn52600685). Scripts used for data analysis are available at GitHub (https://github.com/odufva/nk-bloodcancer). This paper analyzes existing, publicly available data. The accession numbers for the datasets are listed in the key resources table.

EXPERIMENTAL MODEL AND STUDY PARTICIPANT DETAILS

Cell lines

PL-21, GDM-1, SKM-1, and OCI-M1 cells were cultured in IMDM medium (Gibco) with 10% heat-inactivated fetal bovine serum (FBS), 2 mM L-glutamine, and 100 U/ml penicillin with 100 mg/ml streptomycin (PS). All other cell lines were cultured in R10 medium: RPMI-1640 with 10% FBS, 2 mM L-glutamine, and PS. All cultures were incubated at 37°C with 5% CO_2.

PRISM cell line pools were cultured in phenol red-free RPMI 1640 medium with 20% FBS and PS.

KHYG1 cells were cultured in RPMI-1640 with 10% FBS (20% for first passage upon thawing as per manufacturer's instructions), 1% PS and 100 IU/ml of human recombinant IL-2 (R&D Systems, 202-IL-050). Cells were used at low passage numbers, in order to avoid the outgrowth of growth factor independent subclones.

To generate SpCas9-expressing K562, SUDHL4, NALM6, and MOLM14 cells, the cells were transduced with virus produced using the lentiCas9-EGFP plasmid (a gift from Phil Sharp & Feng Zhang, Addgene plasmid # 63592), single-cell sorted using a Sony SH800 cell sorter, and a clone with high and uniform EGFP expression was selected for screening. The MM1.S-SpCas9+ cells were generated and kindly gifted by the laboratory of Dr Benjamin Ebert (DFCI). KMS11-SpCas9+ cells and LP1-SpCas9+ cells (transduced with pLX 311-Cas9 construct, Addgene plasmid # 96924) were obtained from the Broad Institute. MM1.S, KMS11, and LP1 cells were transduced with the lentiviral construct dCAS-VP64_Blast (Addgene plasmid # 61425) for CRISPR activation screens.

Luciferase-expressing K562 (K562-luc) cells were generated using the pLenti PGK V5-LUC Neo (w623-2) construct as previously described for NALM6 (NALM6-luc)[18] The generation of luciferase-expressing SUDHL4 (SUDHL4-luc) cells has been previously described.[18]

All cell lines were STR profiled and tested for Mycoplasma using the MycoAlert kit (Lonza).

Primary NK cell isolation and expansion

Expansion with feeder cells

NK cells were expanded using K562-mbIL21-41BBL feeder cells (CSTX-002, provided by Kiadis, a Sanofi Company) as previously described.[23] Briefly, PBMCs were isolated from buffy coats of healthy donors using Ficoll-Paque gradient centrifugation. Buffy coats were obtained from the Finnish Red Cross Blood Service in accordance with the Declaration of Helsinki and the Helsinki University Hospital ethics committee (permit number 303/13/03/01/2011). Five million PBMCs were suspended in 40 ml R10 supplemented with 10 ng/ml recombinant human IL-2 (R&D Systems, 202-IL-050) together with 10 million K562-mbIL21-41BBL feeder cells irradiated with 100 Gy. Cells were passaged twice a week and feeder cells were added in a 1:1 ratio after 7 days. After 14 days of culture, NK cells were purified using the NK Cell Isolation Kit (Miltenyi) and frozen. NK cells from various donors were thawed and cultured for 5 days in R10 + IL-2 prior to genome-scale CRISPR screens (K562, MOLM14, SUDHL4, NALM6). For all multiplexed scRNA-seq and CROP-seq experiments, NK cells were thawed and cultured 3 days prior to the experiments.

Expansion without feeder cells

PBMCs were isolated from consenting healthy donors. Buffy coats were obtained from the Specimen Bank Brigham and Women's Hospital in accordance with the Declaration of Helsinki (study #T0311). CD3+ cells were depleted using the negative selection cocktail RosetteSep (STEMCELL Technologies Inc.) according to the manufacturer's instructions. CD3-negative PBMCs were then seeded in 6-well plates at a density of $1x10^6$ cells/ml in GMP SCGM media (CellGenix) with 10% heat-inactivated FBS, 1% Glutamax, 200 IU/ml of recombinant human IL-2 (R&D Systems, 202-IL-050) and expanded for 10 – 14 days. Expanded NK cells from PBMCs from the same donor (donor NK12) were used in the genome-scale and focused-library screens with MM1.S, LP1, and KMS11 cells and the PRISM screen. Flow cytometry was performed to verify primary NK cell viability, purity (anti-CD56-PECy7 and anti-CD3-FITC), and expression of NKp46 receptor (anti-NKp46-APC).

METHOD DETAILS

Co-culture assays with multiplexed scRNA-seq readout

Experiments and scRNA-seq library preparation

For the experiment involving 26 cell lines from different hematologic cancers, each cell line was plated separately at 500,000 cells/well on a 24-well plate and day 17 feeder cell-expanded NK cells (1:4 effector-to-target ratio) or NK cells directly extracted from PBMCs (1:2 effector-to-target ratio, donor NK1) or only R10 culture medium (targets only) were added, resulting in a total volume of 1 ml R10. Experiments were performed in batches of 13-14 cell lines, and wells with only NK cells were included (Table S1B). After 24 h co-culture, we labeled the cells from each monoculture or co-culture condition with oligonucleotide-conjugated antibodies against ubiquitously expressed surface proteins (with different oligonucleotide for each mono- or co-culture), enabling multiplexing in the scRNA seq using the cell hashing method.[22]

For the time-course experiment, expanded NK cells from donor NK1 were plated at 1:4 effector-to-target ratio with the indicated cell lines as above for 24, 12, 6, 3, 1, and 0 h prior to cell collection and staining with the cell hashing antibodies. For the culture media transfer experiment, expanded NK cells from donor NK1 were first co-cultured at 1:4 effector-to-target ratio with the target cell lines for 24 h (1.25 million NK cells and 5 million target cells in a T-25 flask with a total of 10 ml culture medium) and culture media at 24 h were collected, centrifuged for 5 min at 300 g to pellet remaining cells, and media were added to either untreated NK cells or untreated target cells. After 24 h culture in the presence of the conditioned media, cells were stained with the cell hashing antibodies and processed for scRNA-seq. For the experiment involving CRISPR-targeted cell lines, day 17 feeder cell-expanded NK cells were used at an 1:1 effector-to-target ratio.

After incubation in 37°C and 5% CO_2, cells from each well were washed 2-3 times with 10 ml PBS, resuspended in 100 μl Cell Staining Buffer (BioLegend), 10 μl TruStain FcX blocking reagent (BioLegend) was added, and cells were blocked for 10 min. A unique TotalSeq-A hashing antibody (BioLegend) was added to each sample (1-2 μl/1-2 μg per sample) and cells were incubated for 30 min at +4°C covered from light. Cells were then washed 3-5 times with 3 ml staining buffer and samples were combined in 1 ml staining

buffer, centrifuged, resuspended to PBS + 0.04% bovine serum albumin (BSA) and proceeded to scRNA-seq. The Chromium Single Cell 3'RNAseq run and library preparations were done using the 10x Genomics Chromium Next GEM Single Cell 3' Gene Expression version 3.1 Dual Index chemistry with the modifications described in Stoeckius et al.,[22] https://cite-seq.com/ and according to the slightly improved protocol described in www.biolegend.com/en-us/protocols/totalseq-a-antibodies-and-cell-hashing-with-10x-single-cell-3-reagent-kit-v3-3-1-protocol. Approximately 15,000 cells were targeted per each 10x lane (GEM well) containing hashed samples from 13 cell lines (cultured either alone or with NK cells, with separate GEM wells for each treatment group). Thus, approximately 1,000-1,200 cells were targeted for sequencing from each cell line mono/co-culture. The 3' GEX and Cell Hashing (multiplexing) libraries were sequenced using Illumina NovaSeq 6000 system using read lengths: 28bp (Read 1), 10bp (i7 Index), 10bp (i5 Index) and 90bp (Read 2).

Data analysis

Data preprocessing was performed using 10x Genomics Cell Ranger v6.0.2 pipelines. The 'cellranger mkfastq' was used to produce FASTQ files and 'cellranger count' to perform alignment, filtering, and UMI counting. The Illumina bcl2fastq v2.2.0 was used to run mkfastq and alignment was done against human genome GRCh38. Count matrix for hashtag oligonucleotides (HTO) was generated using the CITE-seq-Count-tool (DOI: 10.5281/zenodo.2590196).[22]

The R package Seurat (v4.0.4)[94] was used for further scRNA-seq data processing. Cells with > 15% mitochondrial gene counts, > 50% or < 5% ribosomal gene transcripts, < 700 UMI counts, or < 300 or > 10,000 detected genes were filtered out. Hashtag oligonucleotide (HTO) demultiplexing to classify cells to samples was performed on centered log-ratio-normalized HTO UMI counts using the HTODemux function in Seurat with a positive quantile of 0.99. Sample IDs based on HTO data were transferred to transcriptome data and only cells classified as singlets based on HTODemux were considered for further analyses. Across the 193 scRNA-seq samples from the experiments using the 26-cell line panel, we obtained a total of 128,621 cells classified as singlets based on hashtag barcodes (666 cells per sample on average), including 13,983 NK cells (104 cells per sample on average) and 114,638 target cells (645 cells per sample on average).

After log-normalization, the highly variable genes were calculated with the FindVariableFeatures function using the ''mean.var.plot'' selection method in Seurat. Data were scaled and the effect of the cell cycle was corrected using the ScaleData function with scores assigned to each cell using the CellCycleScoring function with G2/M and S phase markers provided in Seurat. Clusters were defined using the FindClusters function with resolution set to 0.8 and cell types were annotated using SingleR.[96] Clusters comprising NK cells were identified and subsequent analyses were focused only on expanded or non-expanded NK cells (NK cell clusters) or cancer cells (all other clusters). The UMAP dimensionality reduction[95] with default parameters was calculated using RunUMAP with the top 20 principal components (PCs).

For the analysis focusing on NK cells (either expanded or non-expanded NK cells), data were re-scaled and the cell cycle effect and batch (resulting from performing the experiments in two batches) were corrected for using the ScaleData function in Seurat. To identify the clusters shown in Figure 1B, only expanded NK cells from donor NK 1 (harboring an adaptive NK cell population) were used. Clusters were defined using the FindClusters function with resolution set to 0.3, and the UMAP was calculated from the top 20 PCs. Cells from all other donors (NK2-NK6) were mapped to these clusters using the FindTransferAnchors and MapQuery functions in Seurat. Differentially expressed genes between clusters were obtained with a Student's *t*-test followed by Bonferroni correction using the FindAllMarkers function in Seurat. Marker genes for each cluster were selected from the genes significantly overexpressed in each cluster compared to other clusters based on significance with regard to NK cell biology and listed in Figures 1B and 1G. For Figure 1G, cells were downsampled to 200 cells per cluster and scaled expression levels of selected genes were plotted.

RNA velocity (the abundances of spliced and unspliced reads) were analyzed with velocyto[33] (v 0.17.17) with GRCh38 build with default parameters. The RNA velocity estimates were then analyzed with scVelo[97] (v0.2.5) with the default model (stochastic) with default parameters, and the resulting velocity vector fields were visualized on the precalculated UMAP space of the spliced reads.

For the analysis focusing on cancer cells, differentially expressed genes between NK cell-treated (three different donors=three biological replicates) and untreated cells (two biological replicates) were obtained with a Student's *t*-test followed by Bonferroni correction using the FindMarkers function in Seurat. Multiple testing correction was performed separately for each cell line comparison. For the differential expression analysis across all cell lines (Figure 2B), 1,000 cells were subsampled from the treated and untreated cells. For UMAP visualizations of each individual cell line, data were scaled, the cell cycle effect was regressed out using ScaleData, and small clusters comprising less than 5% of cells (representing misclassified other cell lines) were removed. The UMAP dimensionality reduction with default parameters was calculated from the top 20 principal components. The core NK cell response score was calculated using the AddModuleScore function in Seurat based on the 17 genes induced by co-culture with expanded NK cells in $\geq$ 50% of the cell lines (*B2M*, *HLA-A*, *HLA-B*, *HLA-C*, *HLA-E*, *TAP1*, *TAPBP*, *STAT1*, *IRF1*, *PSMB8, PSMB9, PSME1, PSME2*, *UBE2L6*, *MT2A*, *BST2*, *GNLY*). To identify gene expression programs activated by NK cell attack in subsets of the cell lines, 200 genes most variably induced across the blood cancer cell lines upon co-culture with expanded NK cells were hierarchically clustered using Euclidean distance and ward.D2 linkage (Figure S2A). Out of these genes, selected genes were shown in Figure 2A, including the core NK cell-induced genes (17 genes induced in at least 50% of the cell lines) and other genes induced in subsets of the cell lines grouped based on functional categories. For Figure 2A, the cell lines were ordered based on the $\log_2$ fold change of a score comprising the core NK cell-induced genes, and by cancer type in the order of median core NK-induced signature. The differential expression was plotted as a dot plot with color indicating $\log_2$ fold change between conditions, dot size indicating the negative $\log_{10}$ of adjusted p value, showing only dots where $p < 0.05$ are shown, with circled dots indicating adjusted $p < 0.05$.

Ligand-receptor interactions were evaluated using CellPhoneDB[37] with default parameters from each cell type subsampled to the same number of cells. Interactions were calculated between all NK cell clusters from donor NK1 and each cell line (both untreated and NK cell-treated), and the significant interactions ($p < 0.05$ permutation testing) based on CellPhoneDB were considered for downstream analyses.

To compute the activation scores for the NK cells co-cultured with CRISPR-targeted cell lines, the AddModuleScore function in Seurat was used on the 50 genes most significantly enriched in the activated cluster (cluster 2) in the cell line panel experiment. When NK cells cultured with target cells expressing two different sgRNAs targeting the same gene were available, the NK cells were pooled together for the analysis. Wilcoxon rank sum test was used to compare NK cells cultured with a gene-targeted cell line to those cultured with the same cell line expressing non-targeting control sgRNAs. The normalized activation scores were obtained by subtracting the median activation score of the same cell line control from the activation scores of the NK cells co-cultured with gene-targeted cell lines. The NK cells co-cultured with CRISPR-targeted cell lines were projected onto the previously computed UMAP visualization from the 26 cell line panel experiment using the FindTransferAnchors and MapQuery functions in Seurat.

Cytokine analysis

Culture media were collected from the mono- or co-cultures at 24 h or indicated timepoints in the time course experiments and stored at -70°C. Cytokine multiplex analysis was performed with the Bio-Plex Pro Human Cytokine 27-plex Assay (M500KCAF0Y, BioRad) per the manufacturer's instructions. Samples were analyzed with the Bio-plex 200 system (BioRad). Values outside the calibrated range were marked as the lowest or highest measured value. To identify cytokines whose concentration is increased in the co-cultures compared to cancer or NK cells cultured alone, the median concentration of each cytokine in NK cell monocultures was first added to the cancer cell monocultures to achieve a concentration reflecting that produced by both cell types without their interaction (''artificial co-culture''). The co-culture fold change was then calculated between the actual co-cultures and the artificial co-cultures using the averages of replicate experiments performed using three different NK cell donors (same as in scRNA-seq experiments). In heatmaps, color indicates concentration $\log_2$ fold change between a NK-cancer cell co-culture and the sum of a cell line cultured alone and NK cells cultured alone. For the heatmap in Figure 2A, cytokines were hierarchically clustered using Spearman's correlation distance and ward.D2 linkage.

Pooled PRISM screen of NK cell cytotoxicity against DNA-barcoded cancer cell lines

PRISM is a platform that allows pooled screening of mixtures of cancer cell lines by labeling each cell line with 24-nucleotide barcodes as previously described.[20] Briefly, 70 suspension blood cancer cell lines (Table S3) stably expressing DNA barcode sequences were seeded in 6-well plates in 8 experimental replicates per condition. The cells were incubated in 5 ml PRISM growth medium (RPMI-1640 without phenol red + 20% FBS + PS) for 24 h. At that point, primary NK cells were washed, resuspended in PRISM growth medium and added to the PRISM cells in 4 different E:T ratios 5:1, 2.5:1, 1.25:1, and 0.625:1 (1 ml/well). Control wells were added with the same volume of media only.

After 24 h co-culture, cells from each well were washed with PBS and incubated for 1 hour at 60°C in lysis buffer (1 ml per well), prepared using double-distilled water with 10% PCR buffer (20mM Tris-HCL PH 8.4, 50mM KCL), 0.45% NP40, 0.45% TWEEN and 10% proteinase K. Genomic DNA from cell lysate was amplified, PCR product was hybridized to Luminex beads with covalently attached antisense barcodes, and streptavidin-phycoerythrin addition, washing, and detection on Luminex FlexMap machines was performed as previously described.[20]

Means of the eight experimental replicates of each cell line were calculated for each E:T ratio and percent viability values were obtained by dividing the mean of each E:T ratio with the mean of the untreated control for each cell line multiplied by 100. Area under the curve (AUC) values were calculated with the percent viability values using the AUC function in the DescTools (v0.99.43) R package. Three non-hematological cell lines included in the pool were removed from the analysis, the gastric adenocarcinoma cell lines HUG1N and SNU1 and the Ewing sarcoma cell line CHLA57. Cell lines with incomplete data at some E:T ratios were similarly removed from the analysis, resulting in a total of 63 evaluable cell lines.

Genome-scale CRISPR-Cas9-based gene editing or gene activation screens

We transduced cell lines from BCL (SUDHL4), B-ALL (NALM6), MM (MM1.S, LP1, KMS11), CML (K562), and AML (MOLM14) with either the GeCKO v2 sgRNA library[105] or the Brunello sgRNA library[106] for loss-of-function (LOF) screens (see STAR Methods). MM cell lines were also transduced with the gain-of-function (GOF) Calabrese library[107] in order to uncover genes with low expression at baseline whose overexpression might alter the cancer cell response to NK cells. Pools of transduced tumor cells were then co-cultured with IL-2-expanded donor-derived NK cells for a period ranging from a minimum of 24 hours to up to two weeks (Figure 4A; Table S4). For the KMS11 and LP1 cells, also the KHYG1 NK cell line was used as effectors. After sequencing the sgRNA barcodes, hits were identified using MAGeCK analysis comparing NK-treated cells to untreated cells.

Production of viral particles

CRISPR screens with genome-scale sgRNA libraries Brunello (CRISPR gene editing) and Calabrese (CRISPR activation): Lenti-X-293T cells (Takara Bio) were plated in T-175 culture flasks (0.6×10^6 cells/ml) in DMEM (Life Technologies) with 10% FBS for 24 h. After decanting the cell medium, OPTI-MEM (6 ml) and Lipofectamine 2000 (100 μl; Life Technologies) were added to each flask plus packaging plasmids psPAX2 (20 μg) and MD2.G (10 μg) and plasmid preps of the Brunello sgRNA library or Calabrese sgRNA library (20 μg per prep; lentiGuide-Puro). Plasmid preps for the Brunello and the Calabrese sgRNA libraries were purchased from

Addgene (#73178 and #1000000111). The transfected Lenti-X-293T cells were incubated at 37ºC (20 min), topped up with fresh media (25 ml), and then refreshed again after 16 hours. Viral supernatants were collected after 24 h and stored at -80ºC prior to use.

CRISPR screens with GeCKO v2 genome-scale sgRNA library: The genome-scale GeCKO v2 sgRNA library in the lentiGuide-Puro plasmid[105,108] (a gift from Feng Zhang, Addgene # 1000000049) was amplified using Endura competent cells (Lucigen) according to instructions provided by the Zhang lab and Lucigen as previously described.[18] To produce lentivirus, 10 μg of both A and B library plasmids were transfected into 293FT cells seeded on the previous day at 11.4 million cells/T-225 flask, together with 15 μg of psPAX2 and 10 μg of pCMV-VSV-G using 100 μl Lipofectamine 2000 (Thermo Fisher Scientific) and 200 μl of Plus Reagent (Thermo Fisher Scientific). After 6 h incubation, the culture medium was replaced with 30 ml of DMEM with 10% FBS and 1% BSA. After 60 h, the viral supernatant was harvested, filtered using a 0.45 μm filter, and stored in -70°C.

Lentiviral transductions with sgRNA libraries

Genome-scale CRISPR gene editing screens with Brunello sgRNA library: Transductions of MM1.S, KMS11, and LP1 cells were performed in batches of $5x10^7$ cells per library for three replicates. Cells were incubated (18 h) in cell medium containing polybrene (5 μg/ml; Santa Cruz Biotechnology), 10 mM HEPES (pH 7.4) (Gibco) and viral prep (30 ml) diluted 1:1. Transduced cells were cultured at an initial density of $1x10^6$ cells/ml and were treated with puromycin (1 μg/ml) for up to 5 days additional two days from transduction. After stable transduction, pooled cells were plated at $40x10^6$ cells per flask (T-175, 100 ml) to enable coverage of 500X and were subcultured at three- to four-day intervals to prevent confluence. The cells were treated with primary NK cells in either duplicates or triplicates for 24 h before harvesting the cells.

Genome-scale CRISPR activation screens with Calabrese sgRNA library: Tumor cells (MM1.S, KMS11, and LP1) were transduced in batches of $3x10^7$ cells per sub-library in triplicates. Cells were incubated (18h) in cell medium containing polybrene (4 μg/ml; Santa Cruz Biotechnology), 10mM HEPES (pH 7.4) (Gibco) and viral prep (30 ml) diluted 1:1. Transduced cells were cultured at an initial density of $1x10^6$ cells/ml and were treated with puromycin (1 μg/ml) for up to 7 days additional two days from transduction. After stable transduction, pooled cells were plated at $30x10^6$ cells per flask (T-175, 100 ml) to enable an estimated average coverage of 500 cells per sgRNA and were treated with primary NK cells in either duplicates or triplicates for 24 h before harvesting the cells. The E:T ratio was selected to kill at least 50% of the tumor cells, according to a dose-response curve.

Genome-scale CRISPR gene editing screens with GeCKO v2 sgRNA library (K562, MOL14, SUDHL4, NALM6): The amount of lentivirus used to transduce the cells was first optimized by transducing cells with a range of virus concentrations on a 12-well plate, where in each well 3 million cells were suspended in a total volume of 1 ml containing 0-1000 μl of GeCKO v2 library virus and 8 μg/ml Polybrene. The plate was centrifuged at room temperature at 800 g for 2 h after which virus 8 was washed away. The cells were treated with or without 0.5 μg/ml puromycin (Thermo Fisher Scientific) for 6 days starting 48 h post-transduction. Transduction efficiency was measured after 72 h puromycin treatment using CellTiter-Glo (CTG, Promega) (50 μl of cell suspension + 50 μl CTG), measured with a Fluostar plate reader (BMG Labtech). Luminescence values (after subtracting background signal obtained from the average of wells containing only R10) in puromycin-treated wells at each virus concentration were divided by values of non-puromycin-treated wells. A concentration resulting in 10-20% transduction efficiency was selected to ensure that the majority of the cells receive only one sgRNA.

For the genome-scale screen, > 400 million cells were transduced in 12-well plates. In each well, 3 million cells were suspended in the titrated virus volume achieving 10-20% transduction in a total volume of 1 ml/well topped up with R10 in the presence of 8 μg/ml Polybrene. The plates were centrifuged at room temperature at 800 g for 2 h, after which the virus was washed away. Transduced cells were selected with 0.5 μg/ml puromycin (0.9 μg/ml for K562) for 6 days starting 24 h post-transduction (48 h for NALM6). On day 7 post-transduction (day 8 for NALM6), cells were divided into NK-treated and untreated conditions in T-225 flasks with 120 ml R10 and 60 million target cells, with effector-to-target ratios as listed in Tables S4A and S4B. In some screens, several different effector-to-target ratios were used. The cells were passaged every 2-3 days and cultured for a duration of 4-17 days as listed in Tables S4A and S4B. To maintain sufficient selection pressure, NK cells were added to the cultures 1-2 times during the screens. Approximately 60 million cells were pelleted at the end and at earlier timepoints, frozen in -70 °C, and later thawed for genomic DNA extraction using Blood Maxi Kit (Qiagen).

Next generation sequencing

Genome-scale screens for CRISPR gene editing with Brunello and CRISPR activation with Calabrese sgRNA libraries: Preparation of DNA for next generation sequencing was undertaken using a two-step PCR protocol as previously described.[108] Briefly, DNA was extracted from frozen cell pellets ($3x10^7$ cells; Blood & Cell Culture DNA Maxi Kit, Qiagen) per manufacturer's instructions. DNA concentration was quantified by UV-spectroscopy (NanoDrop 8000; ThermoFisher Scientific). In the first PCR, sgRNA loci were selectively amplified from a total of 160 μg of genomic DNA (10 μg DNA per sample x 16 reactions, 100 μl volume) using primers described in Table S4C and Phusion® High-Fidelity DNA Polymerase (New England Biolabs, Beverly, MA). This provides approximately 300X coverage for sequencing. A second PCR was performed using 5 μl of the pooled Step 1 PCR product per reaction (1 reaction per 10,000 sgRNAs; 100 μl reaction volume) to attach Illumina adaptors and to barcode samples (Table S4C). Primers for the second PCR included a staggered forward primer (to increase sequencing complexity) and an 8bp barcode on the reverse primer for multiplexing of disparate biological samples (Table S4C). PCR replicates were combined, gel normalized (2% w/v) and pooled, and the entire sample was run on a gel for size extraction. The bands containing the amplified and barcoded sgRNA sequences (approximately 350-370 bp) were excised and DNA extracted (QIAquick Gel Extraction Kit, Qiagen). Multiplexed samples were then sequenced at the Molecular Biology Core Facility (Dana-Farber Cancer Institute) and/or The Genomics Platform (Broad Institute) using an Illumina NextSeq 500 (Illumina, San Diego, CA), allowing approximately $4x10^8$ individual reads per multiplexed sample.

Genome-scale screens for CRISPR gene editing with the GeCKOv2 library: Amplicons containing sgRNA sequences were amplified with a 2-step PCR protocol using primers flanking the sgRNA cassette (Table S4C) as previously described.[18] Briefly, the following overhangs were added to the locus-specific primers to make them compatible with the index primers: Adapter1 (before locus specific forward primer 5'- 3'), Adapter2 (before locus specific reverse primer 5'-3'). The first PCR was performed using 1200 ng of sample DNA and the locus-specific primers, with 96 separate amplifications for each sample. After amplification, all reactions were pooled for the second PCR, in which index primers 1 and 2 and seven identical reactions for each sample pool were used, with a unique combination of dual indexes for each of the sample pools. The seven amplified and indexed reactions were pooled together and purified with Agencourt AMPure XP beads twice. Sample pools were sequenced with Illumina HiSeq 2000 System (Illumina) using read length PE100 or NovaSeq 6000 System (Illumina) using read length PE100.

Data analysis

CRISPR screen data were analyzed using MAGeCK v0.5.2 and v0.5.7.[90] Forward direction reads were aligned to the GeCKO v2 library sgRNA sequences using the mageck count function with default parameters. Comparisons across conditions were performed on the resulting sgRNA read count matrix using the mageck test function with default parameters. For the GeCKO v2 screens with the K562, MOLM14, SUDHL4, and NALM6 cells, all NK-treated and untreated samples from different replicates and E:T ratios were respectively pooled together for the MAGeCK test analysis of each cell line. For the Brunello (LOF) and Calabrese (GOF) libraries, forward direction reads were processed with cutadapt to remove 5' staggered primer adapters and 3' adapters. The sgRNA countmatrix was generated by mapping the trimmed sgRNAs to the corresponding sgRNA library of the CRISPR screen, e.g., Calabrese (GOF), Brunello (LOF) and focused sub-libraries using the mageck count function (perfect match) with default parameters. The sgRNA countmatrix for the MM1S Brunello screen was generated using bowtie2 aligner allowing at most one mismatch for a uniquely matching read. Comparisons between the replicates of NK-treated and untreated cells for a given E:T treatment ratio and experiment in MM1S, LP1, KMS11 were performed using the mageck test function. We used a median read count normalization and non-targeting sgRNAs of the respective library as control distribution for the gene-level rank aggregation in mageck.

For Figure 4B, genes with $p < 0.0001$ and absolute value of the $\log_2$ fold change > 0.75 in at least one screen were plotted, showing data from the screen with the highest significance for each gene. The MAGeCK p values were multiplied by the signs of the $\log_2$ fold change for each gene and plotted on the y axis in Figure 4B with dot size indicating the absolute value of the $\log_2$ fold change (for genes with $p < 0.0001$), whereas the genes were ordered in a randomly sampled order on the x axis. Selected genes out of those with $p < 0.0001$ were colored based on their functional categories.

GSEA was run using fgsea[93] on gene lists ranked based on signed MAGeCK p values. For comparison of the NALM6 NK cell screen with CAR T cell screen in the same cells, CAR T cell screen data were downloaded from Table S5 (File S6) in Dufva et al.[18]

CRISPR screens with focused sgRNA library

Sub-genome scale CRISPR gene editing screens to validate determinants of tumor cell response versus resistance to NK cells in a pooled manner were performed using the same reagents and protocols described in the genome-scale *Brunello* section above. Six hundred thirty-five target genes were selected by pooling top hits and biologically relevant hits from our MM cell screens and our solid tumor screens.[21] Olfactory receptor (OR) genes, which are generally not expressed nor considered to influence tumor cell survival and immune responses, were used to establish a control distribution of sgRNAs.[109,110] A total of 4,000 sgRNAs targeting screen hits and OR gene control sgRNAs were cloned into lentiCRISPRv2 (a gift from Feng Zhang, Addgene plasmid # 52961), with an additional G added in the beginning of the sgRNA sequence when indicated (Table S4P).

Target cell lines MM1.S, LP1 and KMS11 were co-cultured with donor-derived, IL-2 expanded NK cells (same donor as genome-scale screens) or left untreated, in three biological replicates at the following E:T ratios: LP1 and KMS11 1:2, while MM1.S were treated at 2:1 in one experiment and 1:1 in a subsequent experiment. After each screen, DNA extraction, PCR amplification, next generation sequencing, and processing of sequencing data were performed as described for genome-scale screens above.

One-sided test for enrichment and depletion of the sgRNAs and sgRNA rank aggregation was performed for each gene using MAGeCK, with default parameter settings. OR genes were used to establish a control distribution of sgRNAs for the rank aggregation procedure.

For validation purposes, only those genes included among the top 200 in each genome-scale screen were included in the analysis per each cell line.

Individual gene validations

Single-guide RNAs targeting genome-scale screen hits and non-targeting control sgRNAs were cloned into lentiCRISPRv2 (a gift from Feng Zhang, Addgene plasmid # 52961), with an additional G added in the beginning of the sgRNA sequence (Table S4P). The individual genes were selected based on biological interest out of the most highly scoring hits, and included known regulators and genes previously not connected to NK cell cytotoxicity. Lentivirus was produced and luciferase-expressing cells were transduced as described above for the GeCKO library virus. Cells were selected using 0.5 μg/ml puromycin (0.9 μg/ml for K562) prior to experiments. CD43-negative NALM6 cells were obtained from lentiCRISPRv2-sg*SPN*-transduced cells by staining the cells with CD43-PE (BD, clone 1G10, Cat # 560199), and sorting using the Sony SH800 cell sorter.

Cytotoxicity assays using a luciferase readout were performed by plating 10,000-20,000 luciferase-expressing target cells harboring each sgRNA were on a 384-well plate alone or with expanded NK cells at 1:2 effector-to-target ratio in a total volume of 25 μl with 3-6 replicate wells. K562 and NALM6 cells were treated with NK cells for 48 h at 1:2 effector-to-target ratio and

SUDHL4 for 72 h at 1:1 effector-to-target ratio. NK cells for the validation experiments shown in Figure 4D were obtained from a single donor (NK10), different from at least one of the genome-wide screen replicates for the corresponding cell line, to achieve donor-independent validation. Plates were incubated at 37 °C and 5% CO_2 for 24, 48, or 72 h, after which 25 μl ONE-Glo reagent was added to each well and luminescence measured with a Pherastar FS plate reader. Raw luminescence values were normalized to the average of replicates of target cells carrying each sgRNA cultured without NK cells. Average log_2 fold changes were calculated between NK-treated and untreated wells for each sgRNA.

Antibody-mediated blockade

NALM6-luc cells expressing *SPN* or control sgRNAs (2 sgRNAs each, 20,000 cells/well on a 384-well plate in triplicates) were treated with anti-CD43 antibody (10 μg/ml, Abcam, clone MEM-59, Cat # ab9088) or isotype control (10 μg/ml, Abcam, clone 15-6E10A7, Cat # ab170190) and cultured alone or with expanded NK cells from three different donors at E:T ratios 1:8, 1:4, 1:2 and 1:1 for 24 h, followed by luciferase assay as described above.

NK cell direct cytotoxicity assay (calcein AM release assay)

Target cells were cultured as described above and collected by centrifugation at 300 g for 5 min. Cells were washed in PBS and labeled with 0.5 μg/ml Calcein AM (Invitrogen #C1430) in Calcein AM DW buffer (R&D systems, #4892-010-02) at 37°C with 5% CO_2 for 30 min. Calcein-loaded cancer cells were washed twice, resuspended in RPMI medium with probenecid (Invitrogen #P36400), and seeded into a 96-well plate at 10,000 cells/well.

MM1.S-dCas9-VP64 cells expressing sgRNAs for CRISPR activation of *MUC1* (2 sgRNAs) or with the 2 non-targeting control sgRNAs were treated with 700 ng/ml of either purified NA/LE mouse anti-human MUC1 blocking Ab (Cell Signaling #4538, VU4H5) or IgG1κ isotype control (Cell Signaling #5415S, G3A1) to validate the resistance induced by *MUC1* overexpression.

MM1.S dCas9 VP64 cells expressing sgRNAs for CRISPR activation of *SELPLG* (2 clones, sgSELPLG.1 and sgSELPLG.2) and the non-targeting controls (sgCtrl.1, sgCtrl.2) were treated with 10 μg/ml of either purified NA/LE anti-CD162 blocking Ab (BD Pharmingen #556052, KPL-1 RUO) or purified NA/LE mouse IgG1κ isotype control (BD Pharmingen #554721) to validate the resistance induced by *SELPLG* overexpression.

After 10 min incubation of the antibodies at 37°C, feeder layer-expanded NK cells from three different healthy donors were added at the following E:T ratios 3:1, 1:1, 1:2 and untreated control and the plates were incubated at 37°C with 5% CO_2 for 3 h. Released calcein AM was detected at excitation and emission wavelengths of 485 and 520 nm, respectively with Microplate reader (FluoStarOmega, BMG Labtech). The percent of tumor cell lysis was calculated according to:

$$\text{Specific lysis}(\%) = [(\text{ER} - \text{SR}) / (\text{MR} - \text{SR})] * 100$$

ER = experimental release, MR = maximal release, SR = spontaneous release.

MR is that of tumor cells with lysis buffer (Triton X-100 at 10%)

Flow cytometry-based NK cell killing assay

NK cell cytotoxicity on luciferase-negative LP1-Cas9 carrying either *FUT8* or *GMDS* LOF sgRNAs or control sgRNAs was measured by flow cytometry. Before experiment set-up, surface fucose levels were measured via fluorescein-conjugated Lens Culinaris Agglutinin (LCA) (Vector, #FL-1041-5) staining (10 μg/ml)[111] in both knockout and control cells (2 sgRNAs per gene and 2 control sgRNAs). To allow head-to-head comparison and correct for potential plating error, LCA negative knockouts were co-cultured at a 1:1 ratio with their respective LCA positive control and either left untreated or co-cultured with NK cells. The effector cells were co-incubated at the E:T ratios of 1:1 or 2:1 at 37 °C, 5% CO_2 for 24 h.

NK cells for the validation experiment shown in Figure 4E were obtained from a single donor (NK2), different from the one used in the genome-wide screen, to achieve donor-independent validation. Triplicate samples were set up for each E:T ratio. After 24 h, cells were stained with LCA fluorescein 10 μg/ml and NKG2D-APC (BD Biosciences, #558071, clone 1D11) 10 μl/test according to previous calibration, and incubated 30 minutes in the dark. After washing, 7-amino-actinomycin D (7-AAD) (BD Biosciences, # 559925, RUO) was added to every well at the final concentration of 1 μg/ml, as recommended by the manufacturer. As controls, target cells or effector cells alone were also stained to measure spontaneous cell death. After exclusion of doublets, dead cells and NKG2D-positive effector cells, LCA-positive and negative cells were gated to compare cell counts after NK cell treatment in the different conditions. Flow cytometry acquisition was conducted on FACSVerse and FACSuite (BD Biosciences), and the data were analyzed using FlowJo software (FlowJo v10.9.0).

Fucosyltransferase pharmacological inhibition

To evaluate the efficacy of pharmacological modulation of surface fucosylation, we treated LP1 cells carrying control sgRNAs with 100 μM of the fucosyltransferase inhibitor 2F-Peracetyl-Fucose (Sigma-Aldrich, #344827-10MG) or DMSO for 72 h as previously reported,[111] and for 7 days and 14 days, changing half of the media every 3 days. Surface fucose expression was measured by LCA staining (Vector, #FL-1041-5) 10 μg/ml.[111] Flow cytometry acquisition was conducted on FACSVerse and FACSuite (BD Biosciences), and the data were analyzed using FlowJo software (FlowJo v10.9.0).

Analysis of CRISPR screen hit mutations and gene expression

Mutations in CRISPR screen hit genes ($p < 0.00005$ and FDR < 0.2 in any of the screens) were queried from cBioPortal with the online tool (https://www.cbioportal.org/) using the following datasets: Chronic Lymphocytic Leukemia (Broad, Nature 2015), Diffuse Large B-Cell Lymphoma (Duke, Cell 2017), Multiple Myeloma (Broad, Cancer Cell 2014), Acute Myeloid Leukemia (TCGA, PanCancer Atlas), Acute Lymphoblastic Leukemia (St Jude, Nat Genet 2016). The gene list with the above mentioned criteria was used as input

and the resulting mutation list containing altered amino acids and the sample matrix containing a list of all samples where 1=altered and 0=unaltered were downloaded in tab-delimited format. Mutations containing "fs", were annotated as frameshift, mutations ending in "*" as stopgain, and others as missense/other. The identified mutations are listed in Table S5.

Processed gene expression data from normal cell types from BLUEPRINT and ENCODE were downloaded from https://github.com/dviraran/SingleR/blob/master/data/blueprint_encode.rda.

Multi-omics correlations with PRISM-based NK cell sensitivity

Genetic subtypes of the cell lines were annotated based on previous studies as listed in Table S3A. A data matrix containing genomic and other multi-omic features was generated for systematic pairwise correlation analyses between PRISM AUC and genomic features in CCLE data. CCLE 2021 quartile 4 data was downloaded from https://depmap.org/portal/download/all/. A feature matrix comprising all available data levels was built, harmonizing sample names by DepMap-ID (columns) and categorizing by features (rows) as numeric or binary. Each feature was annotated as NUMERIC|BINARY:DATATYPE:FEATURE using the following abbreviations: GEXP, gene expression; RPPA, protein expression; METH, methylation; CNVR, copy number variation, GNAB, mutation; MIRN, miRNA; LCMS, metabolomics. In all instances, missing data was reported as NA.

Feature pairs were compared using Spearman's rank correlation followed by p value adjustment using the Benjamini-Hochberg method. In the case of discrete features, only features with at least 5 observations (such as mutations) were used to limit the number of comparisons. Statistical tests were performed to assess whether PRISM-based AUC, as a quantitative metric of the extent of response to NK cells, was correlated with other features, such as gene expression, protein expression, clinical, CNA, mutations, miRNAs, and metabolomics. For genes whose expression correlated with PRISM AUC, the correlation between expression and methylation of the same gene was analyzed. The analyses were performed both across all cell lines and within each cancer type (AML, BCL, B-ALL, T-ALL, MM).

To assess which gene sets were enriched in samples sensitive or resistant to NK cells, GSEA was run using fgsea[93] on gene lists ranked based on signed p values of the correlation with PRISM AUC.

Features identified using the pairwise correlation analyses were visualized at the sample level with heatmaps generated using ComplexHeatmap.[91] The enriched gene sets identified by GSEA were visualized at the sample level using GSVA.[98]

Patient genomic data analysis

Data collection and preprocessing

Feature matrices containing clinical data, processed gene expression values, mutations, CNAs, and subtypes of DLBCL patients from Reddy et al.,[35] Chapuy et al.[99] and the TCGA dataset; MM patients from the CoMMpass dataset[100]; and AML patients from the TCGA dataset[36] preprocessed as previously described[104] were downloaded from Synapse (Reddy et al. DLBCL: https://www.synapse.org/#!Synapse:syn21995529, Chapuy et al. DLBCL: https://www.synapse.org/#!Synapse:syn21991358, TCGA DLBCL: https://www.synapse.org/#!Synapse:syn21995730, CoMMpass MM: https://www.synapse.org/#!Synapse:syn21995455, TCGA AML: https://www.synapse.org/#!Synapse:syn21995719.

Clinical data, processed gene expression values, mutations, and subtypes of 262 T-ALL patients were downloaded from supplementary tables 1, 5, 8, and 15, respectively, from the Liu et al. study.[52]

Processed methylation beta values of 109 T-ALL patients and 20 samples of normal thymocytes were downloaded from GEO (GSE155333). Genetic subtypes were obtained from supplementary table 6 from the Roels et al. study.[53]

Pairwise correlation analysis and visualization

Data matrices containing genomic and other multi-omic features as well as clinical annotations were generated as described above for systematic pairwise correlation analyses, including correlations with the NK cell sensitivity signatures (Figure 5) and with expression of CRISPR screen hits in patient data (Figures 4 and S5). To find patient samples with similar molecular phenotypes as the NK-sensitive cell lines, NK cell sensitivity signatures were obtained by taking 50 genes most significantly correlating with sensitivity to NK cells based on PRISM AUC. The 50 genes were used to calculate an enrichment score of the NK sensitivity signature for each patient sample using GSVA. The NK cell sensitivity signatures were derived separately from MM, T-ALL, and BCL cell lines for use in the corresponding patient datasets. Spearman's rank correlation followed by p value adjustment using the Benjamini-Hochberg method was used to assess whether the NK cell sensitivity signatures were correlated with other features, such as gene expression, clinical, CNAs, or mutations. A similar approach was used to test if the expression of CRISPR screen hits correlated with methylation or copy number of the same gene.

To visualize identified associations of CRISPR/PRISM features with patient genomic and clinical data as dot plots, differential expression between a sample group and all other samples was calculated using Wilcoxon rank sum test. For UMAP visualizations, expression values of 15% of the most variable genes were used for dimensionality reduction using the umap R package.[95]

Survival analysis

Univariable survival analyses of CRISPR screen hit gene expression levels were computed with Cox regression using the 'survival' R package (v 3.5-5) in myeloma, AML, and DLBCL datasets (for myeloma GEO: GSE19784, GEO: GSE16716, GEO: GSE24080, CoMMpass; for DLBCL GEO: GSE10846, GEO: GSE11318, GEO: GSE17372, GEO: GSE98588, Reddy et al.; and for AML GEO: GSE10358, GEO: GSE12662, GEO: GSE12417, GEO: GSE14468, GEO: GSE6891, BeatAML, TCGA AML). Processed data from these datasets were downloaded from Synapse (DOI: 10.7303/syn21991014).[103,104] Established prognostic factors, such as International Staging System (ISS) for myeloma and International Prognostic Index (IPI) and ABC/GCB subtypes for DLBCL and age in

AML were also included in the analyses. CRISPR screen hits with $p < 0.0001$ and absolute value of the $\log_2$ fold change > 0.75 in at least one CRISPR screen were included in the analysis. Genes with a significant univariable survival association at 5% FDR in at least one cohort were included in the final results.

Single-cell transcriptomics CRISPR screens

Experiments and preparation of scRNA-seq libraries

To generate lentiviral sgRNA libraries for single-cell CRISPR screens, guides targeting screen hits (three sgRNAs for each gene) and non-targeting control sgRNAs (four for K562, six for other screens; Table S7A) were cloned into CROPseq-Guide-Puro (a gift from Christoph Bock, Addgene # 86708)[54] or into CROP-sgRNA-MS2 (a gift from Wolf Reik, Addgene # 153457).[112] Lentivirus was produced and cells stably expressing Cas9 or dCas9-VP64 were transduced as described above using different concentrations of virus. Cells were selected with puromycin (0.5 μg/ml for K562, SUDHL4, and NALM6; 1 μg/ml for MM1.S, LP1, and KMS11) and cells transduced with a concentration resulting in a 10-20% transduction efficiency based on a viability assay described above were selected for screening. Target cells were co-cultured with day 17 feeder cell-expanded NK cells for 24 h at 1:16 and 1:4 effector-to-target ratios (only 1:16 for K562) or left untreated, and both conditions were subjected to scRNA-seq after washing twice with 10 ml PBS + 0.04% BSA.

The Chromium Single Cell 3' RNAseq run and library preparation were done using the 10x Genomics Chromium Next GEM Single Cell 3' Gene Expression v3.0 chemistry (K562), v3.1 chemistry (SUDHL4, NALM6, MM1.S), or v3.1 Dual Index chemistry (LP1, MM1.S CRISPRa). CROP-seq guide sequencing libraries were prepared using nested PCRs described in Hill et al.[113] and https://github.com/shendurelab/single-cell-ko-screens#enrichment-pcr. Briefly, 13 ng of full length 10x cDNA was used as template for the first round of amplification. The subsequent 2nd and 3rd PCR reactions were done using SPRIselect Reagent (1.0X) purified and 1:25 diluted PCR product as template. Optimal amplification cycles were selected based on quantitative PCR analysis. The guide sequencing libraries were sequenced alongside the 3' GEX libraries with approximately 10% read depth when compared to 3' GEX libraries. The K562, SUDHL4, NALM6, and MM1.S sample libraries were sequenced on Illumina NovaSeq 6000 system using the following read lengths: 28bp (Read 1), 8bp (i7 Index), 0 bp (i5 Index) and 89bp (Read 2). The LP1 and MM1.S CRISPRa sample libraries were sequenced on Illumina NovaSeq 6000 system using the following read lengths: 28bp (Read 1), 10bp (i7 Index), 10bp (i5 Index) and 90bp (Read 2).

Data analysis

Data preprocessing was performed using 10x Genomics Cell Ranger v3.1 (K562, SUDHL4, NALM6, MM1.S) or v6.0.2 (LP1, MM1.S CRISPRa) pipelines. The 'cellranger mkfastq' function was used to produce FASTQ files and 'cellranger count' to perform alignment, filtering, and UMI counting. The Illumina bcl2fastq v2.2.0 was used to run mkfastq function and alignment was done against the human genome GRCh38.

FASTQ files of the targeted sgRNA amplification libraries were run through Cell Ranger count v3.1.0 pipeline. UMI counts of guides associated with each cell were extracted using the get_barcodes.py script[113] downloaded from https://github.com/shendurelab/single-cell-ko-screens. To assign guides to cells, cells harboring sequences with > 10 UMI counts and accounting for > 50% of the UMI counts in the cell were included in the analysis. Out of these, cells in which the second most frequent guide accounted for > 20% of the UMI counts were considered to express two guides and were removed from the analysis.

The R package Seurat (v4.0.4)[94] was used for further scRNA-seq data processing. Cells with > 10-15% mitochondrial gene counts, > 50% or < 5% ribosomal gene transcripts, < 3,000 UMI counts, or < 300 or > 10,000 detected genes were filtered out. After log-normalization, the highly variable genes were calculated with the FindVariableFeatures function in Seurat using the 'vst' selection method. Data were scaled, clusters were defined based on PCs with a standard deviation > 2 using the FindNeighbors and FindClusters functions, and cell types were annotated using SingleR. Clusters comprising NK cells, doublets, or low-quality cells were removed. The sgRNA–cell assignments were merged with the expression object, which was subsetted to cells assigned a single sgRNA. Differential expression between cells expressing guides targeting a gene and non-targeting controls or between untreated or NK cell-treated control sgRNA-carrying cells was performed with a Student's *t*-test using the FindMarkers function in Seurat with logfc.threshold = 0.1. Multiple testing correction using the Bonferroni method was performed separately for each perturbation. Similarity of the differential expression gene lists across perturbations was assessed using the CompareLists function in the OrderedList package (v1.64.0).

The mixscape tool in Seurat was used to detect perturbations with a transcriptomic phenotype and visualize their relative differences as previously described.[55] CalcPerturbSig was used to calculate perturbation signatures reflecting the perturbation-specific differences between cells expressing gene-targeting guides and cells expressing control guides, and cells were classified as perturbed or non-perturbed using RunMixscape with logfc.threshold = 0.025 and gene.count = 5. Cells classified as non-perturbed were removed from the analysis and the similarity of the perturbations was visualized as a UMAP based on linear discriminant analysis computed using the MixscapeLDA function.

The core NK cell response score was calculated as described above and differential enrichment of the score in various perturbations was calculated with the Student's *t*-test using the FindMarkers function in Seurat similarly as for genes.

Comparison with patient data

For the genes perturbed in CROP-seq experiments and mutated in at least 5 patients with either MM (CoMMpass), DLBCL (Reddy et al.), or AML (TCGA), differential expression between tumor cells from patients with versus without mutations were determined using limma.[114] Genes significantly differentially expressed in the same direction at a nominal p value threshold of 0.05 in both CROP-seq and in patients when the same gene was knocked out or mutated, respectively, were identified.

QUANTIFICATION AND STATISTICAL ANALYSIS

Detailed information on the statistical method for all quantitative data was described in each method paragraph, and is reported in figure legends, and figures. The Spearman's correlation was used for the statistical analysis between two numeric variables. The non-parametric two-sided Wilcoxon rank sum test or the unpaired two-sided Welch's t-test was used for statistical analysis between two groups. P value between multiple groups was obtained using a Kruskal-Wallis test and p values between each pair using Wilcoxon rank sum tests followed by Benjamini-Hochberg (BH) adjustment. For CRISPR single gene validation (luciferase-based, flow cytometry and calcein AM release assays), p values were obtained using an unpaired t-test with Welch's correction. In case other statistical tests were used, all information is provided in the figure legend. Only p values for significant pairs are shown (* < 0.05, ** < 0.01, *** < 0.001, **** < 0.0001)